

1 **ACSL3 is a novel GABARAPL2 interactor that links ufmylation and**  
2 **lipid droplet biogenesis**

3  
4 Franziska Eck<sup>1</sup>, Santosh Phuyal<sup>3</sup>, Matthew D. Smith<sup>4</sup>, Manuel Kaulich<sup>2</sup>, Simon  
5 Wilkinson<sup>4</sup>, Hesso Farhan<sup>3</sup>, and Christian Behrends<sup>1</sup>

6  
7 <sup>1</sup>Munich Cluster for Systems Neurology (SyNergy), Medical Faculty, Ludwig-Maximilians-  
8 University München, Feodor-Lynen Strasse 17, 81377 Munich, Germany

9 <sup>2</sup>Institute of Biochemistry II, Goethe University School of Medicine, Theodor-Stern-Kai 7, 60590  
10 Frankfurt am Main, Germany

11 <sup>3</sup>Institute of Basic Medical Sciences, Department of Molecular Medicine, University of Oslo,  
12 Sognsvannsveien 9, 0372 Oslo, Norway

13 <sup>4</sup>Cancer Research UK Edinburgh Centre, MRC Institute of Genetics and Molecular Medicine,  
14 University of Edinburgh, U.K., EH4 2XR

15 **Correspondence to:** christian.behrends@mail03.med.uni-muenchen.de

16  
17 **Running title:** CRISPR/Cas9-tagging of hATG8s

18  
19 **Keywords:** GABARAPL2, ACSL3, lipid droplets, UBA5, ufmylation, ER-phagy

28 **Abstract** (180 words)

29 While studies of ATG genes in knockout models led to an explosion of knowledge about the  
30 functions of autophagy components, the exact roles of LC3 and GABARAP proteins are still  
31 poorly understood. A major drawback for their understanding is that the available interactome  
32 data was largely acquired using overexpression systems. To overcome these limitations, we  
33 employed CRISPR/Cas9-based genome-editing to generate a panel of cells in which human  
34 ATG8 genes were tagged at their natural chromosomal locations with an N-terminal affinity  
35 epitope. This cellular resource was exemplarily employed to map endogenous GABARAPL2  
36 protein complexes using interaction proteomics. This approach identified the ER-associated  
37 protein and lipid droplet (LD) biogenesis factor ACSL3 as a stabilizing GABARAPL2-binding  
38 partner. GABARAPL2 bound ACSL3 in a manner dependent on its LC3-interacting regions  
39 whose binding site in GABARAPL2 was required to recruit the latter to the ER. Through this  
40 interaction, the UFM1-activating enzyme UBA5 became anchored at the ER. Further, ACSL3  
41 depletion and LD induction affected the abundance of several ufmylation components and ER-  
42 phagy. Together, we describe ACSL3 as novel regulator of the enigmatic UFM1 conjugation  
43 pathway.

44

45

46

47

48

49

50

51

52

53

54

55

56

## 57 **Introduction**

58 From yeast to humans ATG8s are highly conserved proteins. While there is only a single Atg8  
59 in yeast, the human ATG8 (hATG8) family is subdivided into the orthologs microtubule-  
60 associated protein 1A/1B light chain 3 (MAP1LC3) including LC3A, LC3B, and LC3C as well  
61 as  $\gamma$ -aminobutyric acid receptor-associated protein (GABARAP) including GABARAP,  
62 GABARAPL1 and GABARAPL2 (Slobodkin and Elazar, 2013). All six hATG8 proteins share  
63 the same, ubiquitin-like fold although they do not exhibit any sequence homologies with  
64 ubiquitin. However, within and between the ATG8 subfamilies, the amino acid sequences show  
65 high similarities (Shpilka et al., 2011). A major feature of LC3 and GABARAP proteins is their  
66 covalent conjugation to the phospholipid phosphatidylethanolamine (PE). This process is  
67 initiated by the cysteine proteases ATG4A-D that cleave all hATG8 family members to expose  
68 a C-terminal glycine residue and is followed by the activation of LC3s and GABARAPs through  
69 the E1-like activating enzyme ATG7. PE-conjugation of hATG8 proteins is subsequently  
70 accomplished in a concerted action of the E2-like conjugating enzyme ATG3 and the E3-like  
71 ligase scaffold complex ATG12-ATG5-ATG16L1. PE-hATG8 conjugates are reversible  
72 through cleavage by ATG4A-D (Mizushima et al., 2011).

73 The best understood function of hATG8s is in macroautophagy (hereafter referred to as  
74 autophagy) which is a highly conserved degradation pathway that eliminates defective and  
75 unneeded cytosolic material and is rapidly upregulated by environmental stresses such as  
76 nutrient deprivation. In the past years, it was shown that autophagy is capable of selectively  
77 recognizing and engulfing diverse cargo such as aggregated proteins (aggrephagy), pathogens  
78 (xenophagy) or mitochondria (mitophagy) with the help of specific receptor proteins (Kirkin and  
79 Rogov, 2019). Initiation of autophagy leads to the formation of phagophores (also called  
80 isolation membranes) from preexisting membrane compartments, such as the ER. Elongation  
81 and closure of isolation membranes leads to engulfment of cargo inside double membrane  
82 vesicles termed autophagosomes. Fusion of autophagosomes with lysosomes forms  
83 autolysosomes in which captured cargo is degraded in bulk by lysosomal hydrolases (Dikic  
84 and Elazar, 2018). During this process, GABARAPs and LC3s are associated with the outer  
85 and inner membrane of phagophores and regulate membrane expansion (Xie et al., 2008),  
86 cargo receptor recruitment (Stolz et al., 2014), closure of phagophores (Weidberg et al., 2011)  
87 and the fusion of autophagosomes with lysosomes (Nguyen et al., 2016).

88 Besides autophagy, GABARAPs and LC3s are implicated in a number of other cellular  
89 pathways. For example, GABARAP was found as interactor of the GABA receptor and involved  
90 in its intracellular transport to the plasma membrane (Leil et al., 2004, Wang et al., 1999), while  
91 GABARAPL2 was identified as modulator of Golgi reassembly and intra-Golgi trafficking

92 (Legesse-Miller et al., 1998, Muller et al., 2002). GABARAPs were also found as essential  
93 scaffolds for the ubiquitin ligase CUL3<sup>KBTBD6/KBTBD7</sup> (Genau et al., 2015). Among others, LC3s  
94 have regulatory functions in RhoA dependent actin cytoskeleton reorganization (Baisamy et  
95 al., 2009) as well as in the regulation of ER exit sites (ERES) and COPII-dependent ER-to-  
96 Golgi transport (Stadel et al., 2015). This high functional diversity of GABARAPs and LC3s  
97 implies that these proteins are more than autophagy pathway components and that there are  
98 possible other unique functions of individual hATG8 proteins to be unraveled.

99 So far, interactome and functional analyses of LC3s and GABARAPs were mostly done in cells  
100 overexpressing one of the six hATG8 family members (Behrends et al., 2010, Popovic et al.,  
101 2012). This raises the concern that an overexpressed hATG8 protein might take over functions  
102 or interactions of one of the other family members due to their high sequential and structural  
103 similarity. A lack of isoform specific antibodies further complicates the analysis of distinct  
104 functions of hATG8s. To facilitate the study of endogenous GABARAPs and LC3s, it is  
105 important to generate alternative resources and tools such as the multiple hATG8 knockout  
106 cell lines (Nguyen et al., 2016) or the hATG8 family member-specific peptide sensors (Stolz et  
107 al., 2017). To circumvent the hATG8 antibody problem, we used CRISPR/Cas9 technology to  
108 seamlessly tag hATG8 genes at their natural chromosomal locations. The generated cell lines  
109 (hATG8<sup>endoHA</sup>) express N-terminally hemagglutinin (HA)-tagged hATG8 family members at  
110 endogenous levels and are a powerful tool to study the functions of individual GABARAPs and  
111 LC3s. All created cell lines were tested for their correct sequence and functionality. As a proof  
112 of concept, we performed interaction proteomics with the GABARAPL2<sup>endoHA</sup> cell line and  
113 characterized the interaction with the novel binding partner ACSL3.

114

## 115 **Results**

### 116 *Establishment of cells carrying endogenously HA tagged LC3s and GABARAPs*

117 Complementary to our previously reported LC3C<sup>endoHA</sup> HeLa cell line (Le Guerroue et al., 2017)  
118 we sought to employ CRISPR-mediated gene-editing to generate a panel of cells in which the  
119 remaining five hATG8 family members are seamlessly epitope tagged at their natural  
120 chromosomal locations. To this end, we directed Cas9 to cleave DNA at the vicinity of the start  
121 codon of LC3 and GABARAP genes in order to stimulate microhomology-mediated integration  
122 of a sequence encoding for a single HA-tag using a double-stranded DNA donor molecule  
123 containing short homology arms (Kaulich and Dowdy, 2015). Briefly, we designed PCR  
124 homology templates in which the blasticidine resistant gene, a P2A sequence and the open  
125 reading frame of the HA-tag were flanked by homology arms to the 5'UTRs and first exons of  
126 the LC3/GABARAP genes (Fig. S1A). In parallel, we designed single guide RNAs (sgRNAs)



127 for all hATG8 genes except LC3C and cloned them into pX330, a SpCas9 expressing vector  
128 (Fig. S1A). We then transfected HeLa cells with corresponding pairs of homology template and  
129 sgRNA for each LC3/GABARAP gene. After selection with blasticidine, single cell clones were  
130 SANGER sequenced to confirm seamless and locus-specific genomic insertion of the HA-tag.  
131 While we obtained correct clones for GABARAP, GABARAPL1, GABARAPL2 and LC3B (Fig.  
132 S1B), cells that received the homology template and sgRNA for LC3A did not survive the  
133 antibiotic selection. We assume that this is due to the lack of LC3A in HeLa cells as it is  
134 reported that LC3A expression is suppressed in many tumor cell lines (Bai et al., 2012).  
135 Immunoblot analysis of the sequence-validated clones and the parental cells revealed the  
136 presence of the HA-tag in the engineered cell lines that corresponded to the size of the tagged  
137 LC3/GABARAP protein (Fig. 1A, Fig. S2A-C). Gene specific CRISPR/Cas9-editing was further  
138 confirmed by RNAi-mediated depletion of endogenous LC3 or GABARAP proteins in the  
139 corresponding HA-tagged hATG8 cell lines (Fig. 1B, Fig. S2D-F). Consistently, confocal  
140 microscopy of GABARAPL2<sup>endoHA</sup> cells showed a substantially decreased HA immunolabeling  
141 upon knockdown of GABARAPL2 (Fig. 1C). Next, we examined the integrity of the tagged  
142 LC3/GABARAP proteins by monitoring their conjugation to PE in response to treatment with  
143 small molecule inhibitors which either increase lipidation (Torin1), block autophagosomal  
144 degradation (Bafilomycin A1 (BafA1)) or prevent ATG8-PE conjugate formation (ATG7  
145 inhibitor). As expected, GABARAPL2<sup>endoHA</sup>, GABARAP<sup>endoHA</sup> and LC3B<sup>endoHA</sup> cell lines showed  
146 treatment-specific lipidation levels of the respective tagged hATG8 protein (Fig. 1D; Fig.  
147 S2G,I). We also detected lipidated GABARAPL1, though in a manner that was independent  
148 from induction or blockage of autophagy (Fig. 3E). However, as expected autophagy induction  
149 robustly decreased HA-GABARAPL1 protein levels in GABARAPL1<sup>endoHA</sup> cells while blockage  
150 of autophagosomal degradation led to the opposite phenotype (Fig. S2H). Next, we analyzed  
151 the subcellular distribution of one of the HA-tagged hATG8 proteins (i.e. GABARAPL2) in basal  
152 and autophagy-modulating conditions using confocal microscopy. In GABARAPL2<sup>endoHA</sup> cells,  
153 HA-GABARAPL2 was indeed found to colocalize with the autophagosomal and -lysosomal  
154 markers p62, LC3B and LAMP1 and this colocalization increased upon combination treatment  
155 with Torin1 and BafA1 (Fig. 1E-G). Together, we successfully engineered cell lines to carry  
156 epitope tagged hATG8 family members which retain their functionality.

157

### 158 *Mapping the endogenous GABARAPL2 interactome*

159 Next, we selected GABARAPL2<sup>endoHA</sup> cells for a proof-of-principle immunoprecipitation (IP)  
160 followed by mass spectrometric (MS) analysis to identify new candidate binding partners of a  
161 hATG8 family member at endogenous levels. To distinguish between candidates that bind

162 preferentially to PE-conjugated versus unconjugated GABARAPL2 we treated stable isotope  
163 labeling with amino acids in cell culture (SILAC)-labeled GABARAPL2<sup>endoHA</sup> cells with Torin1  
164 and BafA1 (light) or ATG7 inhibitor (heavy). Equal amounts of heavy and light SILAC cells  
165 were mixed, lysed and subjected to an HA-IP. Immune complexes were eluted and size  
166 separated by gel electrophoresis followed by in-gel tryptic digest, peptide extraction and  
167 desalting prior to analysis by liquid chromatography tandem MS. SILAC labeled parental HeLa  
168 cells differentially treated with Torin1/BafA1 or ATG7 inhibitor served as a negative control. In  
169 duplicate experiments, we identified a total of 168 proteins whose abundances in GABARAPL2  
170 immunoprecipitates were altered by at least 2.8-fold ( $\log_2$  SILAC ratio  $\geq 1.5$  or  $\leq -1.5$ ) in  
171 response to modulation of the GABARAPL2 conjugation status (Fig. 2A). Among these  
172 regulated proteins were well-characterized hATG8 binding proteins such as ATG7, CCPG1  
173 and SQSTM1 (also known as p62) as well as several candidate interactors of LC3 and  
174 GABARAP proteins previously found in large-scale screening efforts such as the mitochondrial  
175 outer membrane protein VDAC1, the nucleoprotein AHNAK2, the translation initiation factor  
176 EIF4G1 and the small GTPase IRGQ (Ewing et al., 2007, Rolland et al., 2014) (Fig. 2A). In  
177 addition, a number of known hATG8 binding proteins including UBA5, HADHA, HADHB,  
178 RB1CC1, TRIM21 and IPO5 was found to bind GABARAPL2 independent of its lipidation  
179 status since these proteins did not display substantial changes in their SILAC ratios.

180

### 181 *ACSL3 is a novel binding partner of GABARAPL2*

182 Since functional annotation analysis using DAVID revealed 'fatty acid metabolism' as a term  
183 previously not associated with LC3/GABARAP-interacting proteins (Fig. S2J), we focused on  
184 the proteins found in this category. In particular, the long-chain-fatty-acid-CoA ligase 3  
185 (ACLS3) attracted our attention as it was the only ER-localized protein among these  
186 candidates. To validate ACSL3 as novel GABARAPL2 interacting protein, we performed HA-  
187 IPs on lysates derived from parental and GABARAPL2<sup>endoHA</sup> cells which were either transiently  
188 transfected with ACSL3-myc, myc-p62 or -ATG7 or left untreated. Notably, p62 and ATG7  
189 served as positive controls. Immunoblotting with epitope tag- and gene-specific antibodies  
190 revealed that overexpressed and endogenous p62 and ATG7 as well as ACSL3 associated  
191 with endogenous GABARAPL2 (Fig. 2B,C). Thus, these results indicate that our hATG8<sup>endoHA</sup>  
192 cells are indeed valuable tools to examine the LC3 and GABARAP interactome at endogenous  
193 levels and to identify novel binding partners such as ACSL3.

194

### 195 *GABARAPL2 is stabilized by ACSL3*

196 Since GABARAPL2 is involved in autophagic cargo engulfment (Schaaf et al., 2016), we tested  
197 whether ACSL3 is an autophagy substrate or serves as selective autophagy receptor.  
198 However, stimulation of GABARAPL2<sup>endoHA</sup> cells with Torin1, BafA1, a combination of both or  
199 with ATG7 inhibitor showed that ACSL3 protein levels did not change upon autophagy  
200 induction or blockage (Fig. 3A). Likewise, depletion of GABARAPL2 had no effects on ACSL3  
201 abundance (Fig. 3B). Thus, these results indicate that ACSL3 is neither a substrate nor a  
202 receptor of autophagy under these conditions. Next, we examined the effects of ACSL3  
203 knockdown on GABARAPL2. Treatment of GABARAPL2<sup>endoHA</sup> cells with two different ACSL3  
204 siRNAs showed a significant decrease of GABARAPL2 protein levels (Fig. 3C). To rule out  
205 that this phenotype is due to a global perturbation of the ER, we probed for the integrity of this  
206 organelle in cells depleted of ACSL3 using immunolabeling with Calnexin and the ER exit site  
207 marker SEC13. However, neither the meshwork appearance nor the exist sites of the ER  
208 showed any overt alterations (Fig. S3A,B). Given the high structural and functional similarity  
209 between LC3 and GABARAP family members we addressed whether ACSL3 depletion  
210 likewise impacts on the protein abundance of the other hATG8 family members. Unexpectedly,  
211 ACSL3 knockdown experiments in GABARAP<sup>endoHA</sup>, GABARAPL1<sup>endoHA</sup> and LC3B<sup>endoHA</sup> cells  
212 did not show any significant reduction in the respective HA-tagged hATG8 proteins (Fig. 3D-  
213 F). In contrast, we found that LC3B protein levels significantly increased upon ACSL3 depletion  
214 (Fig. 3F), suggesting that reduced GABARAPL2 levels might be compensated by increased  
215 expression of LC3B. Intriguingly, we observed that GABARAPL2 protein levels are restored in  
216 RNAi-treated GABARAPL2<sup>endoHA</sup> cells treated with BafA1 to block autophagosomal  
217 degradation but not with the proteasome inhibitor Bortezomib (Btz) (Fig. 3G). Together, these  
218 results indicate that ACSL3 is not degraded by autophagy but rather serves as a specific  
219 stabilizing factor of GABARAPL2 at the ER.

220

#### 221 *GABARAPL2 localizes with ACSL3 at the ER*

222 ACSL3 is one of five acyl-CoA synthetases and catalysis the conjugation of CoA to long chain  
223 fatty acids to form acyl-CoA (Soupene and Kuypers, 2008). Besides ACSL3 was found to  
224 regulate the formation, the size and the copy number of lipid droplets (Fujimoto et al., 2007,  
225 Kassan et al., 2013). Consistent with its cellular role, ACSL3 is inserted with its N-terminal helix  
226 region midway into the lipid bilayer of the ER membrane or integrated into the monolayer of  
227 lipid droplets (LD) while its C-terminal part encompassing the AMP-binding domain is facing to  
228 the cytoplasm (Brasaemle et al., 2004, Ingelmo-Torres et al., 2009, Poppelreuther et al., 2012).  
229 To further validate the GABARAPL2-ACSL3 interaction, we sought to examine the subcellular  
230 localization of both proteins by confocal microscopy. However, as there were no suitable

231 antibodies for immunofluorescence staining of endogenous ACSL3, we gene-edited  
232 GABARAPL2<sup>endoHA</sup> cells to express ACSL3 tagged at its C-terminus with NeonGreen (Fig.  
233 S1A,C). Immunoblot analysis of these newly established GABARAPL2<sup>endoHA</sup>/ACSL3<sup>endoNeonGreen</sup>  
234 cells in comparison with GABARAPL2<sup>endoHA</sup> and parental HeLa cells transfected with TOMM20-  
235 NeonGreen confirmed the correct size of the ACSL3-NeonGreen fusion (approximately 106  
236 kDa; ACSL3 80 kDa + NeonGreen 26 kDa) (Fig. 4A). Colocalization of ACSL3-NeonGreen  
237 with the ER-membrane localized chaperone Calnexin demonstrated that the NeonGreen tag  
238 did not interfere with the ER localization of ACSL3 (Fig. 4B). As ACSL3 is essential for LD  
239 formation, we tested whether the ACSL3-NeonGreen chimera is fully functional. Thereto,  
240 GABARAPL2<sup>endoHA</sup>/ACSL3<sup>endoNeonGreen</sup> cells were treated with oleic acid to induce LD formation  
241 or EtOH as control prior to fixation and labeling of phospholipids and neutral lipids. Confocal  
242 microscopy showed a clear colocalization of ACSL3 with phospholipids and neutral lipids in  
243 control cells while ACSL3 redistributed in the phospholipid monolayer of LDs when cells were  
244 treated with oleic acid for 24 hrs (Fig. 4C). Next, we analyzed fixed and HA-immunolabeled  
245 GABARAPL2<sup>endoHA</sup>/ACSL3<sup>endoNeonGreen</sup> cells by confocal microscopy and super-resolution radial  
246 fluctuations (SRRF) imaging. Consistent with our biochemical experiment, we observed partial  
247 colocalization of endogenous GABARAPL2 and ACSL3 (Fig. 4D). Together, these results  
248 show that NeonGreen tagged ACSL3 is correctly localized at the ER membrane, integrates  
249 into the monolayer of LDs upon free fatty acid treatment and associates with GABARAPL2 at  
250 the ER.

251

### 252 *ACSL3 binds GABARAPL2 in a LIR-dependent manner*

253 Interaction between hATG8 proteins and their binding partners involves an ATG8 family-  
254 interacting motif (AIM; also known as LC3-interacting region (LIR)) in the hATG8 interactors  
255 and the LIR-docking site (LDS) in LC3 and GABARAP proteins (Noda et al., 2008, Pankiv et  
256 al., 2007, Rogov et al., 2014). Amino acid sequence analysis of ACSL3 with iLIR (Kalvari et  
257 al., 2014) and manual inspection revealed four potential LIRs (LIR-1: 65-71, LIR-2: 135-140,  
258 LIR-3: 589-594, LIR-4: 643-648) (Fig. 5A). To determine whether ACSL3 employs at least one  
259 of these sites to bind GABARAPL2 we performed binding experiments with purified GST-  
260 tagged wild-type and a LIR-binding deficient GABARAPL2 mutant in which the relevant amino  
261 acids of the LDS were replaced with alanine (i.e. Y49A/L50A). These two GABARAPL2  
262 variants were incubated with lysates derived from HeLa cells stably expressing full-length  
263 ACSL3 or two fragments thereof. While the first fragment spanned residues 1-85 and included  
264 the ER membrane-binding domain and LIR-1, the second fragment ranged from residues 86-  
265 718 and contained the AMP binding site, LIR-2-4 (Fig. 5A). Immunoblot analysis of the

266 pulldown assay showed binding of wild-type GABARAPL2 to full-length ACSL3 and both of its  
267 fragments (Fig. 5B), indicating that ACSL3 contains at least two distinct binding sites for  
268 GABARAPL2. Intriguingly, GABARAPL2 lacking a functional LDS did not interact with ACSL3  
269 86-718 while it retained binding to the wild-type ACSL3 and fragment 1-85 (Fig 5B). This  
270 suggests that GABARAPL2 employs its LDS to bind to a LIR within residues 86-718 of ACSL3  
271 while GABARAPL2 seem to employ a different binding site to interact with a motif in the  
272 preceding ACSL3 sequence. To start dissecting the relevance of our binding model for the  
273 recruitment of GABARAPL2 to ACSL3 at the ER, we subjected HeLa cells stably expressing  
274 wild-type or LIR-binding deficient GABARAPL2 to subcellular fractionation using differential  
275 centrifugation. Consistent with our finding that ACSL3 binds GABARAPL2 in a LIR-dependent  
276 manner, immunoblot analysis revealed that wild-type GABARAPL2 is found in the ER fraction  
277 but GABARAPL2  $\Delta$ LDS fail to cofractionate with the ER (Fig. 5C, Fig. S4B). Taken together  
278 these results indicate that the ACSL3-GABARAPL2 interaction involves more than one binding  
279 motif and binding site in GABARAPL2 and ACSL3 and that LIR-dependent ACSL3 binding is  
280 required for the ER recruitment of GABARAPL2.

281

#### 282 *ACSL3 anchors UBA5 to the ER membrane*

283 To better understand the biological significance of the GABARAPL2-ACSL3 interaction, we  
284 turned our attention to known GABARAPL2 binding proteins and in particular to the ubiquitin-  
285 like modifier activating enzyme 5 (UBA5) (Komatsu et al., 2004), which was recently shown to  
286 be recruited to the ER membrane in a GABARAPL2-dependent manner (Huber et al., 2019).  
287 By subjecting lysates derived from parental and GABARAPL2<sup>endoHA</sup> cells that were transiently  
288 transfected with myc-UBA5 or left untreated to HA-IPs, we confirmed the GABARAPL2-UBA5  
289 interaction (Fig. 6A) and demonstrated that it occurs at endogenous levels (Fig. 6B). Since  
290 ACSL3 binds GABARAPL2 at the ER membrane, we investigated whether ACSL3 also  
291 colocalizes with UBA5. Indeed, immunolabeling of fixed GABARAPL2<sup>endoHA</sup>/ACSL3<sup>endoNeonGreen</sup>  
292 cells with an anti-UBA5 antibody followed by SRRF imaging showed partially colocalization of  
293 UBA5 and ACSL3 (Fig. 6C). Moreover, when we labeled GABARAPL2<sup>endoHA</sup>/ACSL3<sup>endoNeonGreen</sup>  
294 cells with anti-UBA5 and anti-HA antibodies we also observed triple localization of ACSL3,  
295 GABARAPL2 and UBA5 (Fig. 6D). Next, we examined the effect of GABARAPL2 depletion on  
296 the ACSL3-UBA5 interaction. Thereto, we transfected HeLa cells stably overexpressing  
297 ACSL3-HA with myc-UBA5 and a siRNA against GABARAPL2 or a non-targeting control  
298 followed by HA-IP. Consistent with the notion that GABARAPL2 recruits UBA5 to ACSL3, we  
299 observed a clear reduction of UBA5 levels in ACSL3 immunoprecipitates upon GABARAPL2  
300 knockdown (Fig. 6E). Lastly, we asked whether the ACSL3-UBA5 interaction is modulated by

301 lipid stress. To address this question, we performed myc-IPs on lysates derived from myc-  
302 UBA5-transfected mock or ACSL3-HA expressing HeLa cells that were grown in the absence  
303 and presence of oleic acid. Remarkably, we found that UBA5 associates with ACSL3  
304 independent of its activity during LD formation (Fig. 6F). Overall, these results suggest that  
305 ACSL3, GABARAPL2 and UBA5 form a complex at the ER membrane in dependency of  
306 GABARAPL2.

307

### 308 *ACSL3 regulates ufmylation pathway components*

309 Since we found that ACSL3 stabilizes GABARAPL2, we investigated whether ACSL3 depletion  
310 has similar effects on UBA5 protein abundance. For this purpose, GABARAPL2<sup>endoHA</sup> cells  
311 were transfected with siRNA against ACSL3 or a non-targeting control and grown in the  
312 absence or presence of BafA1 or Btz. Indeed, we observed that protein levels of UBA5  
313 decreased upon ACSL3 depletion but they were not restored by blockage of autophagosomal  
314 or proteasomal degradation (Fig. 7A,B). While depletion of GABARAPL2 had no effects on  
315 UBA5 protein levels (Fig. 3B). This supports the notion that UBA5 and GABARAPL2 form a  
316 functional unit which is regulated by ACSL3. UBA5 is part of the conjugation system, termed  
317 ufmylation, that covalently attaches the ubiquitin-like protein ubiquitin fold modifier 1 (UFM1)  
318 to target proteins through an E1-E2-E3 multienzyme cascade. The E1-like enzyme UBA5  
319 activates UFM1 by forming a thioester bond between its active site and the exposed C-terminal  
320 glycine of UFM1 (Komatsu et al., 2004). The UFM1-conjugating enzyme 1 (UFC1) then  
321 transfers UFM1 from UBA5 to the UFM1-protein ligase 1 (UFL1) which mediates the  
322 attachment to target proteins (Komatsu et al., 2004, Tatsumi et al., 2010). While UFC1 is  
323 cytosolic, the ER-membrane bound protein DDRGK1 anchors UFL1 to the ER membrane (Wu  
324 et al., 2010) and is reported to be one of the few known ufmylation targets besides RPL26  
325 (Walczak et al., 2019), RPN1 (Liang et al., 2019) and ASC1 (Yoo et al., 2014) (Tatsumi et al.,  
326 2010). While the consequences of ufmylation remains poorly understood at the mechanistic  
327 level, the UFM1 conjugation pathway has been linked to the ER stress response (Lemaire et  
328 al., 2011, Zhang et al., 2012), erythrocyte differentiation (Cai et al., 2015, Tatsumi et al., 2011),  
329 cellular homeostasis (Zhang et al., 2015) and breast cancer progression (Yoo et al., 2014).  
330 Since the stability of UBA5 and its ER-recruiting factor GABARAPL2 was controlled by ACSL3,  
331 we probed whether it also regulates the abundance of the other proteins in the ufmylation  
332 cascade. Knockdown experiments revealed that the protein levels of UFL1 and DDRGK1 were  
333 significantly decreased upon ACSL3 depletion while the abundance of UFC1 was significantly  
334 increased. Conjugated UFM1 was largely unchanged (Fig. 7A,B, Fig. S4C). The observation  
335 that the protein levels of UBA5, UFL1 and DDRGK1 were not restored by blockage of

336 autophagy or the proteasome (Fig. 7A,B) indicates that these ufmylation factors are most likely  
337 regulated at the transcriptional level. Together, this suggest that ACSL3 not only anchors UBA5  
338 but might act as novel regulator of the ufmylation cascade.

339

#### 340 *LDs regulate UFM1 conjugation and ER-phagy*

341 The finding that the LD biogenesis factor ACSL3 stabilizes several components of the UFM1  
342 conjugation pathway raises the question whether LD biogenesis and ufmylation are  
343 functionally coupled. To test this hypothesis, we monitored the ufmylation pathway in response  
344 to induction of LD formation in GABARAPL2<sup>endoHA</sup> cells grown in the absence and presence of  
345 oleic acid for 0.5, 4 and 8 hrs, respectively. While UBA5 levels significantly decreased in the  
346 course of 8 hrs oleic acid treatment, there was no effect on UFC1 (Fig. 7C,D). In contrast, the  
347 protein levels of DDRGK1 and UFL1 both decreased in the first 4 hrs of incubation with oleic  
348 acid but after 8 hrs at least DDRGK1 levels were almost restored (Fig. 7C,D). Interestingly, we  
349 detected significantly more conjugated UFM1 (~35 kDa) after 4 hrs of oleic acid incubation  
350 (Fig. S4D) which might be due to altered ufmylation and de-ufmyltion dynamics. Given that LD  
351 formation induced a substantial suppression of several ufmylation components and that these  
352 components was recently shown to be required for starvation-induced, ER sheet-targeting  
353 selective autophagy (Liang et al., 2019), we examined whether induction of LD blocks this ER-  
354 phagy pathway. Thereto, we employed the recent developed ER-autophagy tandem reporter  
355 system which allows the quantification of reticulolysosomes (Liang et al., 2018). Briefly, HeLa  
356 cells were transfected with mCherry-eGFP-RAMP4 and starved with EBSS for 8 hrs in  
357 combination with either EtOH or oleic acid. As expected, we observed a robust decrease in  
358 the numbers of red-only puncta which indicates reduced reticulolysosomes and hence an  
359 inhibition of ER-phagy (Fig. 8A,B). Together, these results indicate that the ufmylation cascade  
360 is differentially regulated during induction of LD and that the ACSL3-GABARAPL2-UBA5 axis  
361 plays an important part in this regulation.

362

## 363 **Discussion**

364 In this study, we identified the ER-associated protein ACSL3 as novel binding partner of  
365 GABARAPL2 and UBA5 using a CRISPR/Cas9 generated GABARAPL2<sup>endoHA</sup> cell line.  
366 Furthermore, we provide evidences for the regulation of ufmylation through ACSL3 and LD  
367 biogenesis.

368 In our interactome screen with endogenously tagged GABARAPL2 we found ACSL3, which  
369 we confirmed as GABARAPL2 interactor by immunoprecipitations, GST pulldowns and SRRF

370 imaging. Moreover, our data suggest, that this interaction is mediated by a LIR and one  
371 additional binding motif in ACSL3. By using GABARAPL2 LIR-binding deficient mutants as well  
372 as N- and C-terminal ACSL3 fragments we narrowed down the LIR in ACSL3 within the amino  
373 acids 86-718, thereby excluding candidate LIR-1. Given that candidate LIR-2 is localized within  
374 the AMP-binding domain of ACSL3 and therefore unlikely accessible, candidate LIR-3 or -4  
375 might mediate the binding to the LDS of GABARAPL2 (Fig. S4A). In addition, our binding  
376 studies indicate a GABARAPL2 LDS-independent binding motif within residues 1-85 of ACSL3.  
377 In addition to the LIR/LDS pairing, Marshall and colleagues recently reported an alternative  
378 hATG8 interaction modus in which binding partners employ a ubiquitin-interacting motif (UIM)  
379 to bind to an UIM-docking site (UDS) in LC3 and GABARAP proteins (Marshall et al., 2015).  
380 According to the UIM consensus sequence (Marshall and Vierstra, 2019) we indeed found a  
381 potential UIM (amino acids 73-81) in ACSL3 by manual sequence inspection (Fig. S4A).  
382 However, this candidate UIM is reversed in its sequence similar to inverted SUMO interaction  
383 motifs (Matic et al., 2010). Whether and how this UIM bind to GABARAPL2's UDS remains to  
384 be structurally determined. Importantly, our subcellular fractionation assay revealed that  
385 GABARAPL2 recruitment to the ER membrane is dependent on the LIR of ACSL3 as the LDS  
386 GABARAPL2 mutant was dramatically reduced in the ER membrane fractions compared to  
387 wild-type GABARAPL2.

388 GABARAP proteins were shown to mediate ER recruitment of UBA5 to bring it in close  
389 proximity to the membrane bound UFM1 E3 enzyme complex composed of UFL1, DDRGK1  
390 and CDK5R3, thereby facilitating ufmylation (Huber et al., 2019). However, since GABARAPs  
391 are not known to be conjugated to PE at the ER, the molecular basis of this recruitment process  
392 was not clear. Here, we provided evidence that ACSL3 function to anchor UBA5 at the ER  
393 membrane. Given that UBA5 employs an atypical LIR to bind both GABARAPL2 and UFM1  
394 and that the latter is able to outcompete GABARAPL2 binding of UBA5 *in vitro* (Habisov et al.,  
395 2016), it is tempting to speculate that GABARAPL2 interacts with UBA5 until UFM1 conjugation  
396 is triggered. In this scenario, GABARAPL2 is a recruiting factor that hands UBA5 over to  
397 ACSL3 (Fig. 8C). However, the binding mode of ACSL3 and UBA5 remains to be explored.

398 While targets of ufmylation are still largely unknown, three of the known UFM1-modified  
399 proteins are linked to the ER. Firstly, UFM1 conjugation of DDRGK1 is essential for the  
400 stabilization of the serine/threonine-protein kinase/endoribonuclease IRE1 (inositol-requiring  
401 enzyme 1) (Liu et al., 2017, Yoo et al., 2014). Secondly, it was shown that the 60S ribosomal  
402 protein L26 (RPL26) is exclusively ufmylated and de-ufmylated at the ER membrane (Walczak  
403 et al., 2019). Thirdly, Ribophorin1 (RPN1), an ER transmembrane protein and part of the  
404 oligosaccharyltransferase complex, is ufmylated in a DDRGK1-dependent manner (Liang et  
405 al., 2019, Kelleher et al., 1992). Overall, emerging evidence points to a role of the UFM1



406 conjugation system as regulator of ER homeostasis, ER stress response and ER remodeling.  
407 Disruption of protein folding and accumulation of unfolded proteins in the ER are hallmarks of  
408 ER stress which leads to the induction of the unfolded protein response (UPR) via one of these  
409 three key factors: IRE1, PKR-like ER protein kinase (PERK) or activating transcription factor 6  
410 (ATF6). Protein degradation, reduction of protein synthesis and enlargement of the ER  
411 capacity are part of the UPR (Karagoz et al., 2019). In different cell lines and animal models,  
412 it was reported that ufmylation is upregulated via IRE1 or PERK upon ER stress, while  
413 depletion of ufmylation components induce the UPR (Gerakis et al., 2019, Lemaire et al., 2011,  
414 Zhang et al., 2015, Zhang et al., 2012, Zhu et al., 2019). Upon re-established ER homeostasis,  
415 ufmylation coordinates the elimination of extended ER membranes through ER-phagy (Liang  
416 et al., 2019, DeJesus et al., 2016).

417 In our present study, we identified LD formation stimulated by oleic acid treatment as novel  
418 regulator of ufmylation. LD biogenesis starts with lens formation, an accumulation of neutral  
419 lipids between the ER membrane leaflets until LDs eventually bud from the ER. The  
420 hydrophobic neutral lipid core of a LD is surrounded by a phospholipid monolayer with the  
421 origin of the outer ER membrane leaflet (Henne et al., 2018). ACSL3 was identified as LD  
422 associated protein and essential for LD biogenesis, expansion and maturation (Fujimoto et al.,  
423 2004, Kassan et al., 2013). During initiation of LD biogenesis ACSL3 is translocated and  
424 concentrated to pre-LDs to drive LD expansion by mediating acyl-CoA synthesis. However,  
425 cells with enzymatically inactive ACSL3 are still able to form LDs, suggesting additional  
426 functions of ACSL3 in LD biogenesis (Kassan et al., 2013, Kimura et al., 2018). Induction of  
427 LD formation induced by oleic acid which requires ACSL3 resulted in a reduction of UBA5,  
428 UFL1 and DDRGK1 protein levels and thus potentially shut down of UFM1 conjugation (Fig.  
429 7C,D, Fig. 8C). Interestingly, depletion of ACSL3 led to a similar phenotype with regard to  
430 these three ufmylation components. Together, these results suggest that ACSL3 regulates  
431 UBA5, DDRGK1 and UFL1 protein levels and therefore ufmylation (Fig. 8C). The observation  
432 that inhibition of proteasomal or lysosomal degradation did not rescue this phenotype suggests  
433 that these components of the ufmylation machinery are probably downregulated at the  
434 transcriptional level. To what extent this involves one of the three UPR factors IRE1, PERK or  
435 ATF6 remains to be examined. Consistent with the recent finding that ER-phagy is blocked by  
436 inhibition of the interaction between DDRGK1 and UFL1 (Liang et al., 2019), we observed that  
437 LD biogenesis inhibits the remodeling of ER membranes by ER-phagy. While DDRGK1 protein  
438 levels are restored 8 hrs after induction of LD formation it needs to be further investigated when  
439 UFL1 protein levels are reestablished and therefore ER-phagy is restored.

440 Collectively, these findings underline the potential of our CRISPR/Cas9 gene-edited cell lines  
441 to uncover novel cellular pathways involving hATG8 family members without the need of

442 overexpression systems, thereby complementing the recently generated LC3 and GABARAP  
443 knockout cell lines (Nguyen et al., 2016). Together with the LC3C<sup>endoHA</sup> cell line that we  
444 previously reported (Le Guerroue et al., 2017), this cellular resource circumvents the drawback  
445 of unspecific LC3 and GABARAP antibodies and hence will greatly facilitate the functional  
446 dissection of individual hATG8 proteins.

447

## 448 **Material and Methods**

### 449 **Cell culture and treatments**

450 HeLa cell lines were cultured in Dulbecco's modified Eagle's medium (DMEM) + GlutaMAX-I  
451 (Gibco) supplemented with 10 % fetal bovine serum (FBS) and 1mM sodium pyruvate (Gibco)  
452 and grown at 37° C and 5 % CO<sub>2</sub>. For SILAC mass spectrometry, cells were grown in lysine-  
453 and arginine-free DMEM (Gibco) supplemented with 10 % dialyzed FBS, 2 mM glutamine  
454 (Gibco), 1 mM sodium pyruvate (Gibco) and 146 mg/ml light (K0, Sigma) or heavy L-lysine  
455 (K8, Cambridge Isotope Laboratories) and 84 mg/ml light (R0, Sigma) or heavy L-arginine  
456 (R10, Cambridge Isotope Laboratories). SILAC labeled cells were counted after harvesting,  
457 mixed 1:1 and stored at -80° C. For selection Puromycin (2 µg/ml) or Blastidicine (4 µg/ml) was  
458 added to the growth medium. The following reagents were used for treatments: oleic acid (EMD  
459 Millipore, 4954, 600 µm in EtOH, 0.5, 4, 8 or 24 hrs), Bafilomycin A1 (Biomol, Cay11038-1,  
460 200 nM in DMSO, 2 hrs), Torin 1 (Tocris, 4247, 250 nM in DMSO, 2 hrs), Bortezomib (LC Labs  
461 B-1408, 1 µM in PBS, 8 hrs), ATG7 inhibitor (Takeda ML00792183, 1 µM in DMSO, 24 hrs),  
462 EBSS (Sigma E2888, 8 hrs), Doxycycline hyclate (Sigma D9891, 4 µg/ml, 24 hrs).

463

### 464 **Plasmids and stable cell lines**

465 attB flanked ORFs, generated by PCR were cloned into the Gateway entry vector pDONR233.  
466 ORFs from pDONR233 constructs were introduced into one of the following destination vectors  
467 using recombination cloning: pHAGE-N-Flag-HA, pHAGE-C-FLAG-HA, pET-60-DEST,  
468 pEZYmyc-HIS (Addgene, #18701) or pDEST-myc. Stable HA-GABARAPL2 and ACSL3-HA  
469 expressing cells were generate by lentiviral transduction followed selection with 2 µg/ml  
470 Puromycin. pEZY and pDEST constructs were used for transient expression in cells (see  
471 transfection).

472

### 473 **Site directed mutagenesis**

474 For site directed mutagenesis, primers were designed with Quick Change Primer Design  
475 software (Agilent Technologies). First, forward and reverse primers were used in individual  
476 PCR reactions using KOD Hot Start polymerase (Merck Millipore), according to the instruction  
477 of the manufacturer, with the appropriate pDONOR-ORF plasmid as template. In a second  
478 step, PCR reactions were combined and plasmids with the mutated ORF was generated  
479 through a second round of PCR. The obtained PCR mixture was purified with QIAquick PCR  
480 Purification Kit (Qiagen, 28104) and mutated plasmids were amplified in E. coli. Mutagenesis  
481 was verified by sequencing the purified plasmid.

482

### 483 **Genome editing**

484 The N-terminal HA-tagged hATG8 cell lines were generated with homology PCR templates  
485 containing 87 bp of GABARAP/GABARAPL1/GABARAPL2/LC3B-5'UTR including the start  
486 codon followed by the Blastidine resistance gene, P2A, HA and 92bp downstream of the start  
487 codon of the corresponding hATG8 gene. For the C-terminal ACSL3-NeonGreen cell line, we  
488 used a homology PCR template containing 75 bp of the last exon of ACSL3, the NeonGreen  
489 ORF (Allele Biotech), T2A and the Blastidine resistance gene ending with 84 bp downstream  
490 of the last exon of ACSL3. sgRNAs for hATG8s and ACSL3, designed with the online design  
491 tool from the Broad Institute (<https://portals.broadinstitute.org/gpp/public/analysis-tools/sgrna-design>)  
492 were clone into BSbl digested px330 (Addgene #42230), a SpCas9 expressing  
493 plasmid (sgRNA: GABARAP: GGAGGATGAAGTTCGTGTAC, GABARAPL1:  
494 TGCGGTGCATCATGAAGTTC, GABARAPL2: CCATGAAGTGGATGTTCAAG, LC3B:  
495 AGATCCCTGCACCATGCCGT, ACSL3: AGAAAATAATTATTCTCTTC). HeLa cells were  
496 seeded in a 6-well plate and transfected with Lipofectamin 2000 according to the  
497 manufacturer's instructions with sgRNA and corresponding homology PCR template. 48 hrs  
498 later cells were selected with 4 µg/ml Blastidine and subjected to single cell selection in 96-  
499 well plates. Cells with mNeonGreen insertion were FACS sorted. Correct introduction of the  
500 tag was verified by PCR and sequencing.

501

### 502 **Antibodies and dyes**

503 For immunoblotting the following primary antibodies were used at a concentration of 1:1000 in  
504 5 % milk-TBS-T or 5 % BSA-TBS-T or 0.2 % I-Block-TBS-T: ACSL3 (Santa Cruz, sc-166374),  
505 alpha-Tubulin (Abcam, ab64503), ATG7 (Cell Signaling, 8558), Calnexin (Cell Signaling,  
506 2433), c-myc (Bethyl, A190-104A), COXIV (Cell Signaling, 4850), DDRGK1 (Sigma,  
507 HPA013373), GM130 (Abcam, ab52649), HA (Cell Signaling, 3724S/Biolegend, 901501),

508 LaminA/C (Abcam, ab108595), mNeonGreen (Chromotek, 32F6), PCNA (Santa Cruz, sc-  
509 7907), p62 (MBL, PM045/BD, 610832), UBA5 (Proteintech, 12093-1-AP/Sigma, HPA017235),  
510 UFC1 (Proteintech, 15783-1-AP), UFL1 (Abcam, ab226216), UFM1 (Abcam, ab109305) or at  
511 a concentration of 1:100 in 5 % milk-TBS-T: c-myc (Monoclonal Antibody Core Facility,  
512 Helmholtz Zentrum Munich, 9E1, rat IgG1), c-myc (Monoclonal Antibody Core Facility,  
513 Helmholtz Zentrum Munich, 9E10, mouse IgG). As secondary antibodies we used horseradish  
514 peroxidase coupled anti-mouse (Promega, W402B), anti-rabbit (Promega, W401B) and anti-  
515 goat (Dianova, 705035003) antibodies at a concentration of 1:10 000 and anti-rat IgG1  
516 (Monoclonal Antibody Core Facility, Helmholtz Zentrum Munich) antibody at a concentration  
517 of 1:100 in 1 % milk-TBS-T or 1 % BSA-TBS-T or 0.2 % iBlock-TBS-T. The following primary  
518 antibodies and lipid stains were used for immunofluorescence in 0.1 % BSA-PBS: Calnexin  
519 (Stressgen, SPA-860, 1:100), HA (Roche, 11867423001, 1:50), LAMP1 (DSHB, H4A3, 1:50),  
520 LC3 (MBL, PM036, 1:500), p62 (BD, 610832, 1:500), SEC13 (Novus, AF9055-100, 1:300),  
521 HCS LipidTOX™ Red Phospholipidosis Detection Reagent (Thermo Scientific, H34351,  
522 1:1000) and HCS LipidTOX™ Deep Red Neutral Lipid Stain (Thermo Scientific, H34477,  
523 1:500). The following fluorophore conjugated secondary antibodies from Thermo Fisher were  
524 use at a concentration of 1:1000 in 0.1 % BSA-PBS: anti-mouse IgG Alexa Fluor 488 (A-  
525 11001), anti-rabbit IgG Alexa Fluor 488 (A-11008) and anti-rat IgG Alexa Fluor 647 (A-21247).

526

## 527 **Transfection**

528 For siRNA knockdowns, cells were reversely transfected with Lipofectamine RNAiMax  
529 (Thermo Fisher Scientific) according to the manufacturer's guidance with 30 nM of the following  
530 siRNAs from Dharmacon/Horizon Discovery and harvested 72 hrs after transfection: sictrl  
531 UGGUUUACAUGUUUUCUA, siACSL3#1 UAACUGAACUAGCUCGAAA, siACSL3#2:  
532 GCAGUAAUCAUGUACACAA, siGABARAP GGUCAGUUCUACUUCUUGA, siGABARAPL1  
533 GAAGAAAUAUCCGGACAGG, siGABARAPL2 GCUCAGUUCAUGUGGAUCA, siLC3B  
534 GUAGAAGAUGUCCGACUUA. Plasmids were transiently transfected with Lipofectamine  
535 2000 (Thermo Fisher Scientific) according to the instruction of the manufacturer or with 10 mM  
536 PEI (Polyethylenimine) and cells were collected after 48 hrs.

537

## 538 **Immunoblotting**

539 Cell were lysed in RIPA (50 mM Tris-HCl [pH 7.4], 150 mM NaCl, 0.5 % sodium desoxycholate,  
540 1 % NP-40, 0.1 % SDS, 1x EDTA-free protease inhibitor (Roche), 1x phosphatase inhibitor  
541 (Roche)) for 30 min. After elimination of cell debris by centrifugation, proteins were diluted with

542 3x loading buffer (200 mM Tris-HCl [pH 6.8], 6 % SDS, 20 % Glycerol, 0.1 g/ml DTT, 0.1 mg  
543 Bromophenol blue) and boiled at 95°C. Proteins were size separated by SDS-PAGE with self-  
544 casted 8 %, 10 %, 12 % and 15 % gels followed by protein transfer onto nitrocellulose  
545 membranes (GE Healthcare Life Sciences, 0.45 µm). For better visibility of endogenous HA-  
546 hATG8s membranes were boiled for 5 min in PBS after protein transfer. For GST pulldowns,  
547 equal sample loading was confirmed with 5 min Ponceau staining (0.2 % Ponceau S, 3 %  
548 acetic acid) followed by a 10 min TBS-T washing step. Blots were blocked in TBS-T (20 mM  
549 Tris, 150 mM NaCl, 0.1 % Tween-20) supplemented with 5 % low fat milk (Roth) or 5 % BSA  
550 (Albumin from bovin serum, Sigma) or 0.2 % I-Block protein based blocking reagent (Thermo  
551 Fisher) for 1 hr. Primary antibodies were incubated overnight followed by several wash steps  
552 with TBS-T and incubation with secondary antibodies for 1 hr at room temperature. After  
553 repeated washing, immunoblots were analyzed with Western Lightning Plus ECL (Perkin  
554 Elmer).

555

#### 556 **Immunofluorescence**

557 All steps were carried out at room temperature. Cells growing on glass coverslips in 12-well  
558 plates were fixed with 4 % paraformaldehyde in PBS for 15 min followed by permeabilization  
559 with 0,1 % Triton-X-100 in PBS or 0,1 % Saponin in PBS for 15 min and 1 hr blocking in 1 %  
560 BSA-PBS. First and secondary antibody incubation was done sequentially for 1 hr at room  
561 temperature in 0.1 % BSA-PBS followed by mounting of the coverslips with ProlongGold  
562 Antifade with Dapi (Thermo Fisher). In between each step, cells were washed several times  
563 with PBS. Cells were imaged with a LSM 800 Carl Zeiss microscope using 63x oil-immersion  
564 objective and ZEN blue edition software and analyses with ImageJ (version 1.52).

565

#### 566 **Sample preparation for SRRF imaging**

567 For super-resolution radial fluctuations (SRRF; ref. PMID: 29852248) imaging,  
568 GABARAPL2<sup>endoHA</sup>/ACSL3<sup>endoNeonGreen</sup> cells were seeded on 18 mm diameter coverslips at a  
569 density of  $2 \times 10^5$  per 35 mm dish. Following overnight incubation, cells were fixed with 4 % PFA  
570 for 15 min at room temperature, washed three times with 1x PBS followed by a 5 min additional  
571 washing with 50 mM NH<sub>4</sub>Cl. Permeabilization was performed for 5 min with 0.5 % Triton X-100  
572 and blocking for 40 min in 1 % BSA. Following antibodies were used at room temperature in 1  
573 % BSA for 1 hr. Rabbit polyclonal anti-Calnexin (Abcam, ab22595, 1:500), mouse monoclonal  
574 anti-HA (Sigma, H9658, 1:500) and rabbit polyclonal anti-UBA5 (PTGLab, 12093-a-AP, 1:250).

575

## 576 **Acquisition of SRRF images**

577 Confocal microscopy imaging of immunostained HeLa cells was performed on Andor Dragonfly  
578 spinning disk using a Nikon Ti2 inverted optical microscope (60x TIRF objective (Plan-  
579 APOCHROMAT 60 × /1.49 Oil)). Fluorescence was collected with an EMCCD camera (iXon  
580 Ultra 888, Andor). Images were acquired using SRRF-Stream mode in Fusion (version 2.1,  
581 Andor) with additional 1.5x magnification. Following imaging parameters were used. SRRF  
582 Frame count: 150, SRRF Radiality Magnification: 4x, SRRF Ring Radius: 1.4 px, SRRF  
583 Temporal Analysis: Mean and SRRF FPN correction: 75 frames.

584

## 585 **Immunoprecipitation**

586 Frozen cell pellets from 4x15 cm cell culture plates for mass spectrometry or 2x10 cm cell  
587 culture plate for immunoblotting were lysed in Glycerol buffer (20 mM Tris [pH 7.4], 150 mM  
588 NaCl, 5 mM EDTA, 0.5 % Triton-X-100, 10 % Glycerol, 1x protease inhibitor, 1x phosphatase  
589 inhibitor) for 30 min at 4° C with end-over-end rotation. Lysates were cleared from cell debris  
590 by centrifugation prior to adjustment of protein concentrations between the samples and  
591 overnight immunoprecipitation at 4° C with pre-equilibrated anti-HA-agarose (Sigma) or anti-  
592 c-myc-agarose (Thermo fisher). Agarose beads were washed five times with Glycerol buffer  
593 followed by elution of proteins with 3x loading buffer and boiling of the samples at 95° C.  
594 Samples were then analyzed by SDS-PAGE (self-casted or BioRad's 4-20 % gels) followed by  
595 immunoblotting or in-gel tryptic digestion.

596

## 597 **Mass spectrometry**

598 SDS-PAGE gel lines were cut in 12 equal size bands, further chopped in smaller pieces and  
599 placed in 96 well plates (one band per well). Gel pieces were washed with 50 mM ammonium  
600 bicarbonate (ABC)/50 % EtOH buffer followed by dehydration with EtOH, reduction of proteins  
601 with 10 mM DTT in 50 mM ABC at 56° C for 1 hr and alkylation of proteins with 55 mM  
602 iodacetamide in 50 mM ABC at room temperature for 45 min. Prior to overnight trypsin-digest  
603 (12 ng/ul trypsin in 50 mM ABC, Promega) at 37° C, gel pieces were washed and dehydrated  
604 as before. Peptide were extracted from gel pieces with 30 % acetonitrile/3 % trifluoroacetic  
605 acid (TFA), 70 % acetonitrile and finally 100 % acetonitrile followed by desalting on custom-  
606 made C18-stage tips. Using an Easy-nLC1200 liquid chromatography (Thermo Scientific),  
607 peptides were loaded onto 75 µm x 15 cm fused silica capillaries (New Objective) packed with  
608 C18AQ resin (Reprosil- Pur 120, 1.9 µm, Dr. Maisch HPLC). Peptide mixtures were separated  
609 using a gradient of 5 %–33 % acetonitrile in 0.1 % acetic acid over 75 min and detected on an

610 Q Exactive HF mass spectrometer (Thermo Scientific). Dynamic exclusion was enabled for 30  
611 s and singly charged species or species for which a charge could not be assigned were  
612 rejected. MS data were processed with MaxQuant (version 1.6.0.1) and analyzed with Perseus  
613 (version 1.5.8.4, <http://www.coxdocs.org/doku.php?id=perseus:start>). IP experiments from  
614 GABARAPL2<sup>endoHA</sup> and control parental HeLa cells were performed in duplicates and  
615 triplicates, respectively. Matches to common contaminants, reverse identifications and  
616 identifications based only on site-specific modifications were removed prior to further analysis.  
617 Log2 heavy/light ratios were calculated. A threshold based on a log2 fold change of greater  
618 than 1.5-fold or less than -1.5-fold was chosen so as to focus the data analysis on a smaller  
619 set of proteins with the largest alterations in abundance. Additional requirements were at least  
620 two MS counts, unique peptides and razor peptides as well as absence in IPs from parental  
621 HeLa control cells. For functional annotations, the platform DAVID (<https://david.ncifcrf.gov/>)  
622 was used.

623

#### 624 **Subcellular fractionation**

625 For isolation of the endoplasmic reticulum the Endoplasmic Reticulum Isolation Kit (Sigma,  
626 ER0100) was used and all steps were carried out according to the manufacturer's guidance.  
627 Each sample consisted of cells derived from 4x10 cm cell culture plates.

628

#### 629 **Protein expression and purification**

630 For protein expression and purification, pET-60-DEST plasmids containing wild-type or mutant  
631 versions of GABARAPL2 were transformed in Rosetta E. coli. Bacteria were grown in LB  
632 medium at 37° C at 200 rpm and induced with 1 mM IPTG when an OD600nm of 0.5-0.6 was  
633 reached. After 4 hrs, bacteria were harvested by centrifugation and resuspended in lysis buffer  
634 (150 mM NaCl, 50 mM Tris [pH 8.0], 100 µg/ml Lysozyme, 1 mM PMSF, 1mM DTT) and  
635 sonified at an amplitude of 50 % for 10 min (30 sec sonification/30 sec break). Lysates were  
636 cleared from cell debris by centrifugation and incubated overnight with pre-equilibrated  
637 glutathione Sepharose 4B (GE Healthcare) at 4° C with end over end rotation. Glutathione  
638 beads were washed with 150 mM NaCl, 50 mM Tris [pH 8.0] and GST-proteins were eluted  
639 with 10 mM reduced glutathione in 50 mM Tris [pH 8.0]. GST-proteins were dialyzed overnight  
640 in TBS with Slide-A-Lyzer cassettes (Thermo Fisher). Purified GST-proteins were stored at -  
641 80° C until further usage.

642

643 **Pulldown assay**

644 Glutathione Sepharose 4B beads were always freshly coupled prior to pulldown assay. For  
645 one reaction, 40 µl pre-equilibrated glutathione beads slurry was couple to an appropriate  
646 amount of GST-protein overnight at 4° C with end over end rotation. On the next day protein-  
647 coupled glutathione beads were washed with 150 mM NaCl, 50 mM Tris [pH 8.0]. Cells from  
648 2x10 cm cell culture plates per sample were lysed in 600 µl Glycerol buffer for 1 hr. After  
649 clearance of cell debris by centrifugation lysates were precleared for 1 hr at 4° C with pre-  
650 equilibrated uncoupled glutathione beads prior to the adjustment of protein concentrations. To  
651 ensure equal addition of the different GST-proteins, protein-beads binding was monitored by  
652 serial dilutions on Coomassie (0.1 % Brilliant Blue R, 40 % EtOH, 10 % Acetic acid) stained  
653 acrylamide gels. Accordingly coupled beads were diluted and 40 µl per sample was added.  
654 After overnight incubation at 4° C, beads were washed with Glycerol buffer and boiled for 5  
655 min at 95 ° C.

656

657 **ER-phagy assay**

658 HeLa cells were seeded on glass coverslips in 12-well plates. The next day, cells were  
659 transfected with TETOn-mCherry-GFP-RAMP4 at 500 ng per well with FuGENE® HD  
660 transfection reagent (Promega), using manufacturer's recommendations and in the presence  
661 of 4 µg/ml doxycycline. After 24 hrs, cells were placed into fresh complete DMEM medium and  
662 doxycycline was removed. 40 hrs after initial transfection, cells were starved with EBSS  
663 medium for 8 hrs in the presence of either EtOH or oleic acid. Cells were then fixed with 4 %  
664 paraformaldehyde in PBS, pH 7.2 at room temperature for 10 min, washed 3x 5 min with PBS,  
665 stained with 1/5000 DAPI in the penultimate wash and mounted in Dako fluorescent mounting  
666 medium (Dako) onto glass slides. Images were captured with a Nikon A1R TiE confocal  
667 microscope using a 100x 1.4 NA objective (Nikon Instruments). All confocal images are shown  
668 as z-projections of at least 3 z-steps. All quantifications were performed on a minimum of 90  
669 cells across three biological replicates and the standard error of the mean was determined for  
670 each data set. Cells were single blind scored for red-only puncta (autolysosomes).

671

672 **Data availability**

673 The mass spectrometry proteomics data have been deposited to the ProteomeXchange  
674 Consortium (<http://proteomecentral.proteomexchange.org>) via the PRIDE partner repository  
675 with the dataset identifier PXD016734.



676

## 677 **Statistical analysis**

678 Quantification and statistical analysis were done with imageJ and Phyton (version 3.7).  
679 Statistical significance was calculated with Student's t test and data represent  $\pm$  SEM (standard  
680 error of the mean). Statistical analysis of MS data was done with Perseus.

681

## 682 **Acknowledgement**

683 We would like to thank Vladimir Rogov, Henrick Riemenschneider, Georg Werner and all  
684 members of the Behrends lab for reagents, advice and critical discussion. TetOn-mCherry-  
685 eGFP-RAMP4 was a gift from Jacob Corn (Addgene plasmid #109014).

686

## 687 **Author contribution**

688 FE performed all experiments except SRRF imaging and ER-phagy assessment which was  
689 performed by SP and MDS with advice from HF and SW, respectively. MK provided advice for  
690 CRISPR/Cas9 tagging strategy. FE and CB conceived the study and wrote the manuscript.

691

## 692 **Competing interests**

693 The authors declare that they have no conflict of interest.

694

## 695 **Funding**

696 This work was supported by the Deutsche Forschungsgemeinschaft (German Research  
697 Foundation) within the framework of the Munich Cluster for Systems Neurology (EXC2145 - ID  
698 390857198), the Collaborative Research Center 1177 (ID 259130777) and the project grant  
699 BE 4685/2-1. Hesso Farhan was supported by grants from the Norwegian Cancer Society  
700 (182815, 208015), from the Norwegian Research Council (262717) and from the Rakel go Otto  
701 Kr. Bruun legat. A Cancer Research UK Career Development Fellowship to S.W.  
702 (C20685/A12825) funded this work. M.D.S. was also funded by a BBSRC grant to S.W.  
703 (BB/N000315/1).

704

705 **References**

- 706 BAI, H., INOUE, J., KAWANO, T. & INAZAWA, J. 2012. A transcriptional variant of the LC3A  
707 gene is involved in autophagy and frequently inactivated in human cancers. *Oncogene*, 31,  
708 4397-408.
- 709 BAISAMY, L., CAVIN, S., JURISCH, N. & DIVIANI, D. 2009. The ubiquitin-like protein LC3  
710 regulates the Rho-GEF activity of AKAP-Lbc. *J Biol Chem*, 284, 28232-42.
- 711 BEHRENDTS, C., SOWA, M. E., GYGI, S. P. & HARPER, J. W. 2010. Network organization of  
712 the human autophagy system. *Nature*, 466, 68-76.
- 713 BRASAEMLE, D. L., DOLIOS, G., SHAPIRO, L. & WANG, R. 2004. Proteomic analysis of  
714 proteins associated with lipid droplets of basal and lipolytically stimulated 3T3-L1 adipocytes.  
715 *J Biol Chem*, 279, 46835-42.
- 716 CAI, Y., PI, W., SIVAPRAKASAM, S., ZHU, X., ZHANG, M., CHEN, J., MAKALA, L., LU, C.,  
717 WU, J., TENG, Y., PACE, B., TUAN, D., SINGH, N. & LI, H. 2015. UFBP1, a Key Component  
718 of the Ufm1 Conjugation System, Is Essential for Ufm1-Mediated Regulation of Erythroid  
719 Development. *PLoS Genet*, 11, e1005643.
- 720 DEJESUS, R., MORETTI, F., MCALLISTER, G., WANG, Z., BERGMAN, P., LIU, S., FRIAS,  
721 E., ALFORD, J., REECE-HOYES, J. S., LINDEMAN, A., KELLIHER, J., RUSS, C., KNEHR,  
722 J., CARBONE, W., BEIBEL, M., ROMA, G., NG, A., TALLARICO, J. A., PORTER, J. A.,  
723 XAVIER, R. J., MICKANIN, C., MURPHY, L. O., HOFFMAN, G. R. & NYFELE, B. 2016.  
724 Functional CRISPR screening identifies the ufmylation pathway as a regulator of  
725 SQSTM1/p62. *Elife*, 5.
- 726 DIKIC, I. & ELAZAR, Z. 2018. Mechanism and medical implications of mammalian autophagy.  
727 *Nat Rev Mol Cell Biol*, 19, 349-364.
- 728 EWING, R. M., CHU, P., ELISMA, F., LI, H., TAYLOR, P., CLIMIE, S., MCBROOM-  
729 CERAJEWSKI, L., ROBINSON, M. D., O'CONNOR, L., LI, M., TAYLOR, R., DHARSEE, M.,  
730 HO, Y., HEILBUT, A., MOORE, L., ZHANG, S., ORNATSKY, O., BUKHMAN, Y. V., ETHIER,  
731 M., SHENG, Y., VASILESCU, J., ABU-FARHA, M., LAMBERT, J. P., DUEWEL, H. S.,  
732 STEWART, II, KUEHL, B., HOGUE, K., COLWILL, K., GLADWISH, K., MUSKAT, B., KINACH,  
733 R., ADAMS, S. L., MORAN, M. F., MORIN, G. B., TOPALOGLOU, T. & FIGEYS, D. 2007.  
734 Large-scale mapping of human protein-protein interactions by mass spectrometry. *Mol Syst*  
735 *Biol*, 3, 89.
- 736 FUJIMOTO, Y., ITABE, H., KINOSHITA, T., HOMMA, K. J., ONODUKA, J., MORI, M.,  
737 YAMAGUCHI, S., MAKITA, M., HIGASHI, Y., YAMASHITA, A. & TAKANO, T. 2007.  
738 Involvement of ACSL in local synthesis of neutral lipids in cytoplasmic lipid droplets in human  
739 hepatocyte HuH7. *J Lipid Res*, 48, 1280-92.
- 740 FUJIMOTO, Y., ITABE, H., SAKAI, J., MAKITA, M., NODA, J., MORI, M., HIGASHI, Y.,  
741 KOJIMA, S. & TAKANO, T. 2004. Identification of major proteins in the lipid droplet-enriched  
742 fraction isolated from the human hepatocyte cell line HuH7. *Biochim Biophys Acta*, 1644, 47-  
743 59.
- 744 GENAU, H. M., HUBER, J., BASCHIERI, F., AKUTSU, M., DOTTSCH, V., FARHAN, H.,  
745 ROGOV, V. & BEHRENDTS, C. 2015. CUL3-KBTBD6/KBTBD7 ubiquitin ligase cooperates with  
746 GABARAP proteins to spatially restrict TIAM1-RAC1 signaling. *Mol Cell*, 57, 995-1010.
- 747 GERAKIS, Y., QUINTERO, M., LI, H. & HETZ, C. 2019. The UFMylation System in  
748 Proteostasis and Beyond. *Trends Cell Biol*, 29, 974-986.
- 749 HABISOV, S., HUBER, J., ICHIMURA, Y., AKUTSU, M., ROGOVA, N., LOEHR, F., MCEWAN,  
750 D. G., JOHANSEN, T., DIKIC, I., DOETSCH, V., KOMATSU, M., ROGOV, V. V. & KIRKIN, V.  
751 2016. Structural and Functional Analysis of a Novel Interaction Motif within UFM1-activating  
752 Enzyme 5 (UBA5) Required for Binding to Ubiquitin-like Proteins and Ufm1-Mediated  
753 Ubiquitination. *J Biol Chem*, 291, 9025-41.
- 754 HENNE, W. M., REESE, M. L. & GOODMAN, J. M. 2018. The assembly of lipid droplets and  
755 their roles in challenged cells. *EMBO J*, 37.
- 756 HUBER, J., OBATA, M., GRUBER, J., AKUTSU, M., LOHR, F., ROGOVA, N., GUNTERT, P.,  
757 DIKIC, I., KIRKIN, V., KOMATSU, M., DOTTSCH, V. & ROGOV, V. V. 2019. An atypical LIR

758 motif within UBA5 (ubiquitin like modifier activating enzyme 5) interacts with GABARAP  
759 proteins and mediates membrane localization of UBA5. *Autophagy*, 1-15.

760 INGELMO-TORRES, M., GONZALEZ-MORENO, E., KASSAN, A., HANZAL-BAYER, M.,  
761 TEBAR, F., HERMS, A., GREWAL, T., HANCOCK, J. F., ENRICH, C., BOSCH, M., GROSS,  
762 S. P., PARTON, R. G. & POL, A. 2009. Hydrophobic and basic domains target proteins to lipid  
763 droplets. *Traffic*, 10, 1785-801.

764 KALVARI, I., TSOMPANIS, S., MULAKKAL, N. C., OSGOOD, R., JOHANSEN, T., NEZIS, I.  
765 P. & PROMPONAS, V. J. 2014. iLIR: A web resource for prediction of Atg8-family interacting  
766 proteins. *Autophagy*, 10, 913-25.

767 KARAGOZ, G. E., ACOSTA-ALVEAR, D. & WALTER, P. 2019. The Unfolded Protein  
768 Response: Detecting and Responding to Fluctuations in the Protein-Folding Capacity of the  
769 Endoplasmic Reticulum. *Cold Spring Harb Perspect Biol*, 11.

770 KASSAN, A., HERMS, A., FERNANDEZ-VIDAL, A., BOSCH, M., SCHIEBER, N. L., REDDY,  
771 B. J., FAJARDO, A., GELABERT-BALDRICH, M., TEBAR, F., ENRICH, C., GROSS, S. P.,  
772 PARTON, R. G. & POL, A. 2013. Acyl-CoA synthetase 3 promotes lipid droplet biogenesis in  
773 ER microdomains. *J Cell Biol*, 203, 985-1001.

774 KAULICH, M. & DOWDY, S. F. 2015. Combining CRISPR/Cas9 and rAAV Templates for  
775 Efficient Gene Editing. *Nucleic Acid Ther*, 25, 287-96.

776 KELLEHER, D. J., KREIBICH, G. & GILMORE, R. 1992. Oligosaccharyltransferase activity is  
777 associated with a protein complex composed of ribophorins I and II and a 48 kd protein. *Cell*,  
778 69, 55-65.

779 KIMURA, H., ARASAKI, K., OHSAKI, Y., FUJIMOTO, T., OHTOMO, T., YAMADA, J. &  
780 TAGAYA, M. 2018. Syntaxin 17 promotes lipid droplet formation by regulating the distribution  
781 of acyl-CoA synthetase 3. *J Lipid Res*, 59, 805-819.

782 KIRKIN, V. & ROGOV, V. V. 2019. A Diversity of Selective Autophagy Receptors Determines  
783 the Specificity of the Autophagy Pathway. *Mol Cell*, 76, 268-285.

784 KOMATSU, M., CHIBA, T., TATSUMI, K., IEMURA, S., TANIDA, I., OKAZAKI, N., UENO, T.,  
785 KOMINAMI, E., NATSUME, T. & TANAKA, K. 2004. A novel protein-conjugating system for  
786 Ufm1, a ubiquitin-fold modifier. *EMBO J*, 23, 1977-86.

787 LE GUERROUE, F., ECK, F., JUNG, J., STARZETZ, T., MITTELBRONN, M., KAULICH, M. &  
788 BEHREND, C. 2017. Autophagosomal Content Profiling Reveals an LC3C-Dependent  
789 Piecemeal Mitophagy Pathway. *Mol Cell*, 68, 786-796 e6.

790 LEGESSE-MILLER, A., SAGIV, Y., PORAT, A. & ELAZAR, Z. 1998. Isolation and  
791 characterization of a novel low molecular weight protein involved in intra-Golgi traffic. *J Biol*  
792 *Chem*, 273, 3105-9.

793 LEIL, T. A., CHEN, Z. W., CHANG, C. S. & OLSEN, R. W. 2004. GABAA receptor-associated  
794 protein traffics GABAA receptors to the plasma membrane in neurons. *J Neurosci*, 24, 11429-  
795 38.

796 LEMAIRE, K., MOURA, R. F., GRANVIK, M., IGOILLO-ESTEVE, M., HOHMEIER, H. E.,  
797 HENDRICKX, N., NEWGARD, C. B., WAELKENS, E., CNOP, M. & SCHUIT, F. 2011. Ubiquitin  
798 fold modifier 1 (UFM1) and its target UFBP1 protect pancreatic beta cells from ER stress-  
799 induced apoptosis. *PLoS One*, 6, e18517.

800 LIANG, J. H., LINGEMAN, E., LUONG, T., AHMED, S., NGUYEN, T., OLZMANN, J. & CORN,  
801 J. E. 2019. A genome-wide screen for ER autophagy highlights key roles of mitochondrial  
802 metabolism and ER-resident UFMylation. *bioRxiv*.

803 LIANG, J. R., LINGEMAN, E., AHMED, S. & CORN, J. E. 2018. Atlastins remodel the  
804 endoplasmic reticulum for selective autophagy. *J Cell Biol*, 217, 3354-3367.

805 LIU, J., WANG, Y., SONG, L., ZENG, L., YI, W., LIU, T., CHEN, H., WANG, M., JU, Z. &  
806 CONG, Y. S. 2017. A critical role of DDRGK1 in endoplasmic reticulum homeostasis via  
807 regulation of IRE1alpha stability. *Nat Commun*, 8, 14186.

808 MARSHALL, R. S., LI, F., GEMPERLINE, D. C., BOOK, A. J. & VIERSTRA, R. D. 2015.  
809 Autophagic Degradation of the 26S Proteasome Is Mediated by the Dual ATG8/Ubiquitin  
810 Receptor RPN10 in Arabidopsis. *Mol Cell*, 58, 1053-66.

811 MARSHALL, R. S. & VIERSTRA, R. D. 2019. Dynamic Regulation of the 26S Proteasome:  
812 From Synthesis to Degradation. *Front Mol Biosci*, 6, 40.

813 MATIC, I., SCHIMMEL, J., HENDRIKS, I. A., VAN SANTEN, M. A., VAN DE RIJKE, F., VAN  
814 DAM, H., GNAD, F., MANN, M. & VERTEGAAL, A. C. 2010. Site-specific identification of  
815 SUMO-2 targets in cells reveals an inverted SUMOylation motif and a hydrophobic cluster  
816 SUMOylation motif. *Mol Cell*, 39, 641-52.

817 MIZUSHIMA, N., YOSHIMORI, T. & OHSUMI, Y. 2011. The role of Atg proteins in  
818 autophagosome formation. *Annu Rev Cell Dev Biol*, 27, 107-32.

819 MULLER, J. M., SHORTER, J., NEWMAN, R., DEINHARDT, K., SAGIV, Y., ELAZAR, Z.,  
820 WARREN, G. & SHIMA, D. T. 2002. Sequential SNARE disassembly and GATE-16-GOS-28  
821 complex assembly mediated by distinct NSF activities drives Golgi membrane fusion. *J Cell*  
822 *Biol*, 157, 1161-73.

823 NGUYEN, T. N., PADMAN, B. S., USHER, J., OORSCHOT, V., RAMM, G. & LAZAROU, M.  
824 2016. Atg8 family LC3/GABARAP proteins are crucial for autophagosome-lysosome fusion but  
825 not autophagosome formation during PINK1/Parkin mitophagy and starvation. *J Cell Biol*, 215,  
826 857-874.

827 NODA, N. N., KUMETA, H., NAKATOGAWA, H., SATOO, K., ADACHI, W., ISHII, J., FUJIOKA,  
828 Y., OHSUMI, Y. & INAGAKI, F. 2008. Structural basis of target recognition by Atg8/LC3 during  
829 selective autophagy. *Genes Cells*, 13, 1211-8.

830 PANKIV, S., CLAUSEN, T. H., LAMARK, T., BRECH, A., BRUUN, J. A., OUTZEN, H.,  
831 OVERVATN, A., BJORKOY, G. & JOHANSEN, T. 2007. p62/SQSTM1 binds directly to  
832 Atg8/LC3 to facilitate degradation of ubiquitinated protein aggregates by autophagy. *J Biol*  
833 *Chem*, 282, 24131-45.

834 POPOVIC, D., AKUTSU, M., NOVAK, I., HARPER, J. W., BEHRENDTS, C. & DIKIC, I. 2012.  
835 Rab GTPase-activating proteins in autophagy: regulation of endocytic and autophagy  
836 pathways by direct binding to human ATG8 modifiers. *Mol Cell Biol*, 32, 1733-44.

837 POPPELREUTHER, M., RUDOLPH, B., DU, C., GROSSMANN, R., BECKER, M., THIELE,  
838 C., EHEHALT, R. & FULLEKRUG, J. 2012. The N-terminal region of acyl-CoA synthetase 3 is  
839 essential for both the localization on lipid droplets and the function in fatty acid uptake. *J Lipid*  
840 *Res*, 53, 888-900.

841 ROGOV, V., DOTSCHE, V., JOHANSEN, T. & KIRKIN, V. 2014. Interactions between  
842 autophagy receptors and ubiquitin-like proteins form the molecular basis for selective  
843 autophagy. *Mol Cell*, 53, 167-78.

844 ROLLAND, T., TASAN, M., CHARLOTEAUX, B., PEVZNER, S. J., ZHONG, Q., SAHNI, N.,  
845 YI, S., LEMMENS, I., FONTANILLO, C., MOSCA, R., KAMBUROV, A., GHIASSIAN, S. D.,  
846 YANG, X., GHAMSARI, L., BALCHA, D., BEGG, B. E., BRAUN, P., BREHME, M., BROLY, M.  
847 P., CARVUNIS, A. R., CONVERY-ZUPAN, D., COROMINAS, R., COULOMBE-  
848 HUNTINGTON, J., DANN, E., DREZE, M., DRICOT, A., FAN, C., FRANZOSA, E., GEBREAB,  
849 F., GUTIERREZ, B. J., HARDY, M. F., JIN, M., KANG, S., KIROS, R., LIN, G. N., LUCK, K.,  
850 MACWILLIAMS, A., MENCHE, J., MURRAY, R. R., PALAGI, A., POULIN, M. M., RAMBOUT,  
851 X., RASLA, J., REICHERT, P., ROMERO, V., RUYSSINCK, E., SAHALIE, J. M., SCHOLZ, A.,  
852 SHAH, A. A., SHARMA, A., SHEN, Y., SPIROHN, K., TAM, S., TEJEDA, A. O., TRIGG, S. A.,  
853 TWIZERE, J. C., VEGA, K., WALSH, J., CUSICK, M. E., XIA, Y., BARABASI, A. L.,  
854 IAKOUCHEVA, L. M., ALOY, P., DE LAS RIVAS, J., TAVERNIER, J., CALDERWOOD, M. A.,  
855 HILL, D. E., HAO, T., ROTH, F. P. & VIDAL, M. 2014. A proteome-scale map of the human  
856 interactome network. *Cell*, 159, 1212-1226.

857 SCHAFF, M. B., KEULERS, T. G., VOOIJS, M. A. & ROUSCHOP, K. M. 2016. LC3/GABARAP  
858 family proteins: autophagy-(un)related functions. *FASEB J*, 30, 3961-3978.

859 SHPILKA, T., WEIDBERG, H., PIETROKOVSKI, S. & ELAZAR, Z. 2011. Atg8: an autophagy-  
860 related ubiquitin-like protein family. *Genome Biol*, 12, 226.

861 SLOBODKIN, M. R. & ELAZAR, Z. 2013. The Atg8 family: multifunctional ubiquitin-like key  
862 regulators of autophagy. *Essays Biochem*, 55, 51-64.

863 SOUPENE, E. & KUYPERS, F. A. 2008. Mammalian long-chain acyl-CoA synthetases. *Exp*  
864 *Biol Med (Maywood)*, 233, 507-21.

865 STADEL, D., MILLARTE, V., TILLMANN, K. D., HUBER, J., TAMIN-YECHESKEL, B. C.,  
866 AKUTSU, M., DEMISHTAIN, A., BEN-ZEEV, B., ANIKSTER, Y., PEREZ, F., DOTSCHE, V.,

867 ELAZAR, Z., ROGOV, V., FARHAN, H. & BEHREND, C. 2015. TECPR2 Cooperates with  
868 LC3C to Regulate COPII-Dependent ER Export. *Mol Cell*, 60, 89-104.  
869 STOLZ, A., ERNST, A. & DIKIC, I. 2014. Cargo recognition and trafficking in selective  
870 autophagy. *Nat Cell Biol*, 16, 495-501.  
871 STOLZ, A., PUTYRSKI, M., KUTLE, I., HUBER, J., WANG, C., MAJOR, V., SIDHU, S. S.,  
872 YOULE, R. J., ROGOV, V. V., DOTSCHE, V., ERNST, A. & DIKIC, I. 2017. Fluorescence-based  
873 ATG8 sensors monitor localization and function of LC3/GABARAP proteins. *EMBO J*, 36, 549-  
874 564.  
875 TATSUMI, K., SOU, Y. S., TADA, N., NAKAMURA, E., IEMURA, S., NATSUME, T., KANG, S.  
876 H., CHUNG, C. H., KASAHARA, M., KOMINAMI, E., YAMAMOTO, M., TANAKA, K. &  
877 KOMATSU, M. 2010. A novel type of E3 ligase for the Ufm1 conjugation system. *J Biol Chem*,  
878 285, 5417-27.  
879 TATSUMI, K., YAMAMOTO-MUKAI, H., SHIMIZU, R., WAGURI, S., SOU, Y. S., SAKAMOTO,  
880 A., TAYA, C., SHITARA, H., HARA, T., CHUNG, C. H., TANAKA, K., YAMAMOTO, M. &  
881 KOMATSU, M. 2011. The Ufm1-activating enzyme Uba5 is indispensable for erythroid  
882 differentiation in mice. *Nat Commun*, 2, 181.  
883 WALCZAK, C. P., LETO, D. E., ZHANG, L., RIEPE, C., MULLER, R. Y., DAROSA, P. A.,  
884 INGOLIA, N. T., ELIAS, J. E. & KOPITO, R. R. 2019. Ribosomal protein RPL26 is the principal  
885 target of UFMylation. *Proc Natl Acad Sci U S A*, 116, 1299-1308.  
886 WANG, H., BEDFORD, F. K., BRANDON, N. J., MOSS, S. J. & OLSEN, R. W. 1999. GABA(A)-  
887 receptor-associated protein links GABA(A) receptors and the cytoskeleton. *Nature*, 397, 69-  
888 72.  
889 WEIDBERG, H., SHPILKA, T., SHVETS, E., ABADA, A., SHIMRON, F. & ELAZAR, Z. 2011.  
890 LC3 and GATE-16 N termini mediate membrane fusion processes required for  
891 autophagosome biogenesis. *Dev Cell*, 20, 444-54.  
892 WU, J., LEI, G., MEI, M., TANG, Y. & LI, H. 2010. A novel C53/LZAP-interacting protein  
893 regulates stability of C53/LZAP and DDRGK domain-containing Protein 1 (DDRGK1) and  
894 modulates NF-kappaB signaling. *J Biol Chem*, 285, 15126-36.  
895 XIE, Z., NAIR, U. & KLIONSKY, D. J. 2008. Atg8 controls phagophore expansion during  
896 autophagosome formation. *Mol Biol Cell*, 19, 3290-8.  
897 YOO, H. M., KANG, S. H., KIM, J. Y., LEE, J. E., SEONG, M. W., LEE, S. W., KA, S. H., SOU,  
898 Y. S., KOMATSU, M., TANAKA, K., LEE, S. T., NOH, D. Y., BAEK, S. H., JEON, Y. J. &  
899 CHUNG, C. H. 2014. Modification of ASC1 by UFM1 is crucial for ERalpha transactivation and  
900 breast cancer development. *Mol Cell*, 56, 261-274.  
901 ZHANG, M., ZHU, X., ZHANG, Y., CAI, Y., CHEN, J., SIVAPRAKASAM, S., GURAV, A., PI,  
902 W., MAKALA, L., WU, J., PACE, B., TUAN-LO, D., GANAPATHY, V., SINGH, N. & LI, H. 2015.  
903 RCAD/Ufl1, a Ufm1 E3 ligase, is essential for hematopoietic stem cell function and murine  
904 hematopoiesis. *Cell Death Differ*, 22, 1922-34.  
905 ZHANG, Y., ZHANG, M., WU, J., LEI, G. & LI, H. 2012. Transcriptional regulation of the Ufm1  
906 conjugation system in response to disturbance of the endoplasmic reticulum homeostasis and  
907 inhibition of vesicle trafficking. *PLoS One*, 7, e48587.  
908 ZHU, H., BHATT, B., SIVAPRAKASAM, S., CAI, Y., LIU, S., KODEBOYINA, S. K., PATEL, N.,  
909 SAVAGE, N. M., SHARMA, A., KAUFMAN, R. J., LI, H. & SINGH, N. 2019. Ufbp1 promotes  
910 plasma cell development and ER expansion by modulating distinct branches of UPR. *Nat*  
911 *Commun*, 10, 1084.

912

## 913 **Figure legends**

914 **Fig. 1. Establishment of cells carrying endogenously HA-tagged LC3s and GABARAPs.**  
915 (A) GABARAPL2<sup>endoHA</sup> and parental HeLa cell lysates were analyzed by immunoblotting using  
916 anti-HA and -PCNA antibodies. The latter was used as loading control. (B,C)

917 GABARAPL2<sup>endoHA</sup> cells were reversely transfected for 72 hrs with non-targeting (sictrl) or  
918 GABARAPL2 siRNA followed by lysis and immunoblot analysis (B) or fixation and  
919 immunolabeling (C) using an anti-HA antibody. Scale bar: 10  $\mu$ m. (D) GABARAPL2<sup>endoHA</sup> cells  
920 were treated as indicated and subjected to lysis and immunoblotting. (E-G) GABARAPL2<sup>endoHA</sup>  
921 cells treated with indicated inhibitors were immunolabeled with anti-p62 (E), anti-LAMP1 (F) or  
922 anti-LC3 (G) antibodies. Scale bar: 10  $\mu$ m. Arrowheads indicate colocalization events.

923

924 **Fig. 2. Endogenous GABARAPL2 interactome.** (A) Scatterplot represents interaction  
925 proteomics of SILAC labeled GABARAPL2<sup>endoHA</sup> cells differentially treated with Torin1 and  
926 BafA1 (light) or ATG7 inhibitor (heavy). Significantly enriched proteins upon Torin1 and BafA1  
927 combination treatment or ATG7 inhibition are highlighted in red and blue, respectively. Proteins  
928 in grey are unchanged. (B,C) Immunoblot analysis of anti-HA immunoprecipitates from lysates  
929 derived from parental HeLa and GABARAPL2<sup>endoHA</sup> cells which were either transiently  
930 transfected for 48 hrs with myc-tagged ATG7, p62 or ACSL3 (B) or left untreated (C).

931

932 **Fig. 3. Stabilization of GABARAPL2 through ACSL3.** (A) GABARAPL2<sup>endoHA</sup> cells were  
933 treated as indicated and subjected to lysis and analyzed with immunoblotting and anti-ACSL3  
934 antibody. (B) Reversely transfected GABARAPL2<sup>endoHA</sup> cells with non-targeting (sictrl) or  
935 GABARAPL2 siRNA were lysed followed by immunoblotting and analysis with indicated  
936 antibodies. (C-F) GABARAPL2<sup>endoHA</sup> (C), GABARAP<sup>endoHA</sup> (D), GABARAPL1<sup>endoHA</sup> (E) and  
937 LC3B<sup>endoHA</sup> (F) cells were reversely transfected with two different ACSL3 siRNAs. Lysates were  
938 analyzed by immunoblotting with indicated antibodies. Data represent mean  $\pm$ SEM. Statistical  
939 analysis (n = 4) of the HA/PCNA ratio normalized to sictrl was performed using Student's t-test  
940 (\*p<0.05, \*\*p<0.01). (G) GABARAPL2<sup>endoHA</sup> cells reversely transfected with siRNAs targeting  
941 ACSL3 for 72 hrs were treated with BafA1 or Btz and analyzed by immunoblotting. Data  
942 represents mean  $\pm$ SEM. Statistical analysis (n = 3) of the HA/PCNA ratio normalized to sictrl-  
943 DMSO, was performed using Student's t-test (\*p<0.05).

944

945 **Fig. 4. Colocalization of GABARAPL2 and ACSL3 at the ER.** (A) GABARAPL2<sup>endoHA</sup> and  
946 GABARAPL2<sup>endoHA</sup>/ACSL3<sup>endoNeonGreen</sup> cells as well as parental HeLa cells transiently  
947 transfected with TOMM20-NeonGreen were lysed and analyzed by immunoblotting with  
948 indicated antibodies. (B), Representative SRRF image of  
949 GABARAPL2<sup>endoHA</sup>/ACSL3<sup>endoNeonGreen</sup> cells immunolabeled with anti-Calnexin. Magnified view  
950 of colocalization events of ACSL3<sup>endoNeonGreen</sup> and the ER marker Calnexin are shown in insets.

951 Scale bars: 5  $\mu$ m. (C) GABARAPL2<sup>endoHA</sup>/ACSL3<sup>endoNeonGreen</sup> cells were treated with oleic acid  
952 or EtOH (control) for 24 hrs followed by fixation and labeling of phospholipids and neutral lipids  
953 with HCS LipidTox lipid stains. Scale bar: 10  $\mu$ m. Two confocal planes are shown for oleic acid  
954 treatment. (D), Representative SRRF image of GABARAPL2<sup>endoHA</sup>/ACSL3<sup>endoNeonGreen</sup> cells  
955 after immunolabeling with anti-HA. Insets show magnified view of colocalization events. Scale  
956 bars: 5  $\mu$ m.

957

958 **Fig. 5. LDS of GABARAPL2 mediate ACSL3 binding and ER recruitment.** (A) Scheme of  
959 wild-type (WT) ACSL3 and fragments with known domains and potential LIRs. (B) Pulldown  
960 assays using GST-tagged WT or  $\Delta$ LBS GABARAPL2 protein incubated with lysates from HeLa  
961 cells expressing WT or fragmented ACSL3 were analyzed by immunoblotting and Ponceau  
962 staining. (D) Subcellular fractionation of HeLa cells stably expressing WT or  $\Delta$ LBS  
963 GABARAPL2 followed by immunoblot analysis with indicated antibodies. PNS, post nuclear  
964 fraction; PMF, post mitochondrial fraction; CMF, crude microsomal fraction.

965

966 **Fig. 6. UBA5 binds to and colocalizes with ACSL3 and GABARAPL2.** (A, B) Immunoblot  
967 analysis of anti-HA immunoprecipitates from lysates derived from parental HeLa and  
968 GABARAPL2<sup>endoHA</sup> cells either transiently transfected for 48 hrs with myc-UBA5 (A) or left  
969 untreated (B) and analyzed with indicated antibodies. (C) Representative SRRF image of  
970 GABARAPL2<sup>endoHA</sup>/ACSL3<sup>endoNeonGreen</sup> cells immunolabeled with anti-UBA5. Colocalization  
971 events of ACSL3<sup>endoNeonGreen</sup> and UBA5 are shown enlarged in insets. Scale bars: 5  $\mu$ m. (D)  
972 Representative SRRF image of GABARAPL2<sup>endoHA</sup>/ACSL3<sup>endoNeonGreen</sup> cells labeled with anti-  
973 HA and -UBA5. Colocalization events of ACSL3<sup>endoNeonGreen</sup>, GABARAPL2<sup>endoHA</sup> and UBA5 are  
974 shown in magnified insets. Scale bars: 5  $\mu$ m. (E) Stable expressing ACSL3-HA cells were  
975 reverse transfected with sictrl or siGABARAPL2 for 72 hrs and transiently transfected with myc-  
976 UBA5 for 48 hrs followed by lysis, anti-HA immunoprecipitation and immunoblot analysis. (F)  
977 Parental HeLa and GABARAPL2<sup>endoHA</sup> cells transfected with myc-UBA5 were treated with oleic  
978 acid or EtOH for 24 hrs prior to lysis, anti-myc immunoprecipitation and immunoblotting.

979

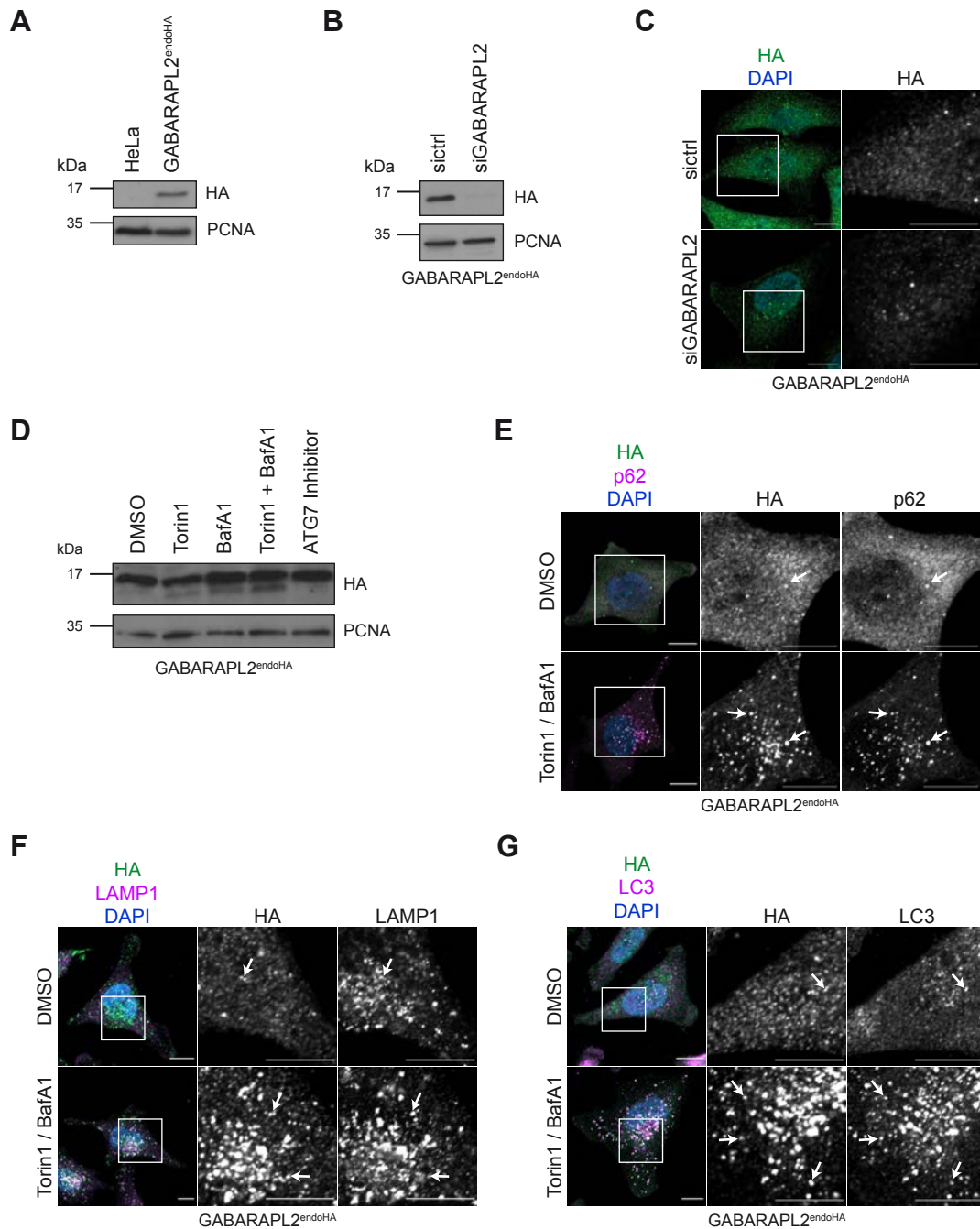
980 **Fig. 7. ACSL3 and LD biogenesis regulate the ufmylation pathway.** (A) GABARAPL2<sup>endoHA</sup>  
981 cells were transfected with ACSL3 siRNAs and treated with Btz or BafA1 followed by lysis and  
982 immunoblot analysis using indicated antibodies. (B) Quantitative analysis of A. Data represents  
983 mean  $\pm$ SEM. Statistical analysis (n = 3) of the indicated protein/PCNA ratio normalized to sictrl-  
984 DMSO was performed using Student's t-test (\*p<0.05, \*\*p<0.01, \*\*\*p<0.001). (C)

985 GABARAPL2<sup>endoHA</sup> cells were treated with oleic acid or EtOH for 0.5, 4 or 8 hrs prior to lysis  
986 and immunoblotting with indicated antibodies. (D) Quantitative analysis of C. Data represents  
987 mean  $\pm$ SEM. Statistical analysis (n = 3) of the indicated protein/PCNA ratio normalized to 0.5  
988 hrs EtOH was performed using Student's t-test (\*p<0.05, \*\*p<0.01).

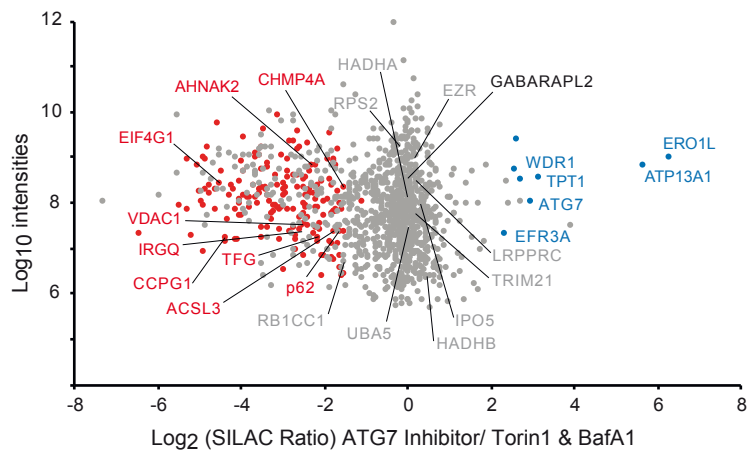
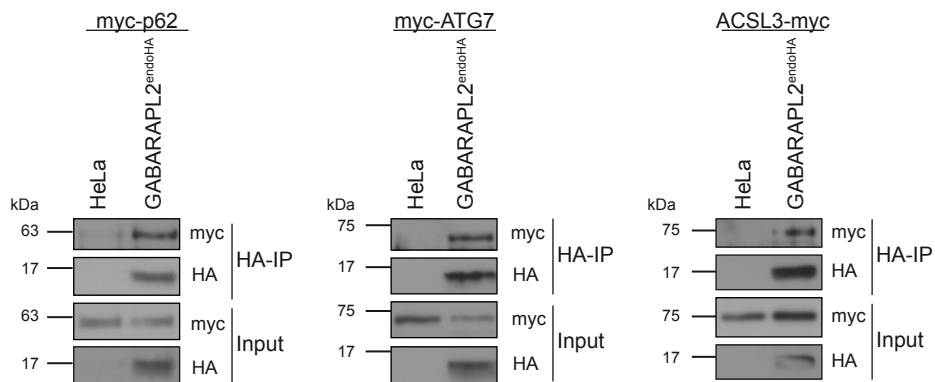
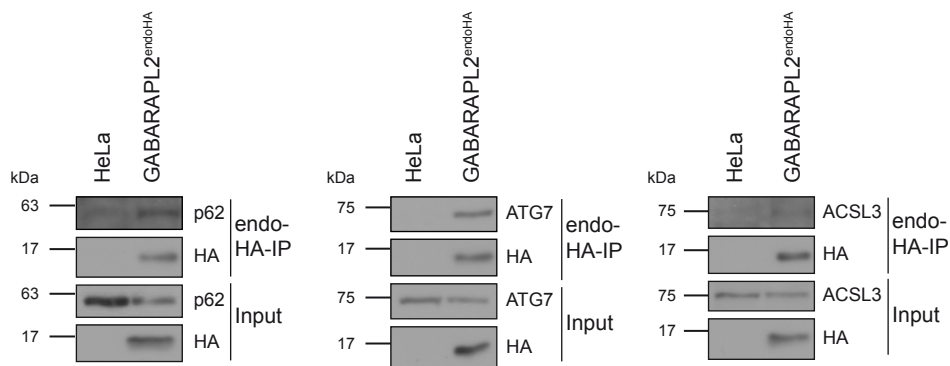
989

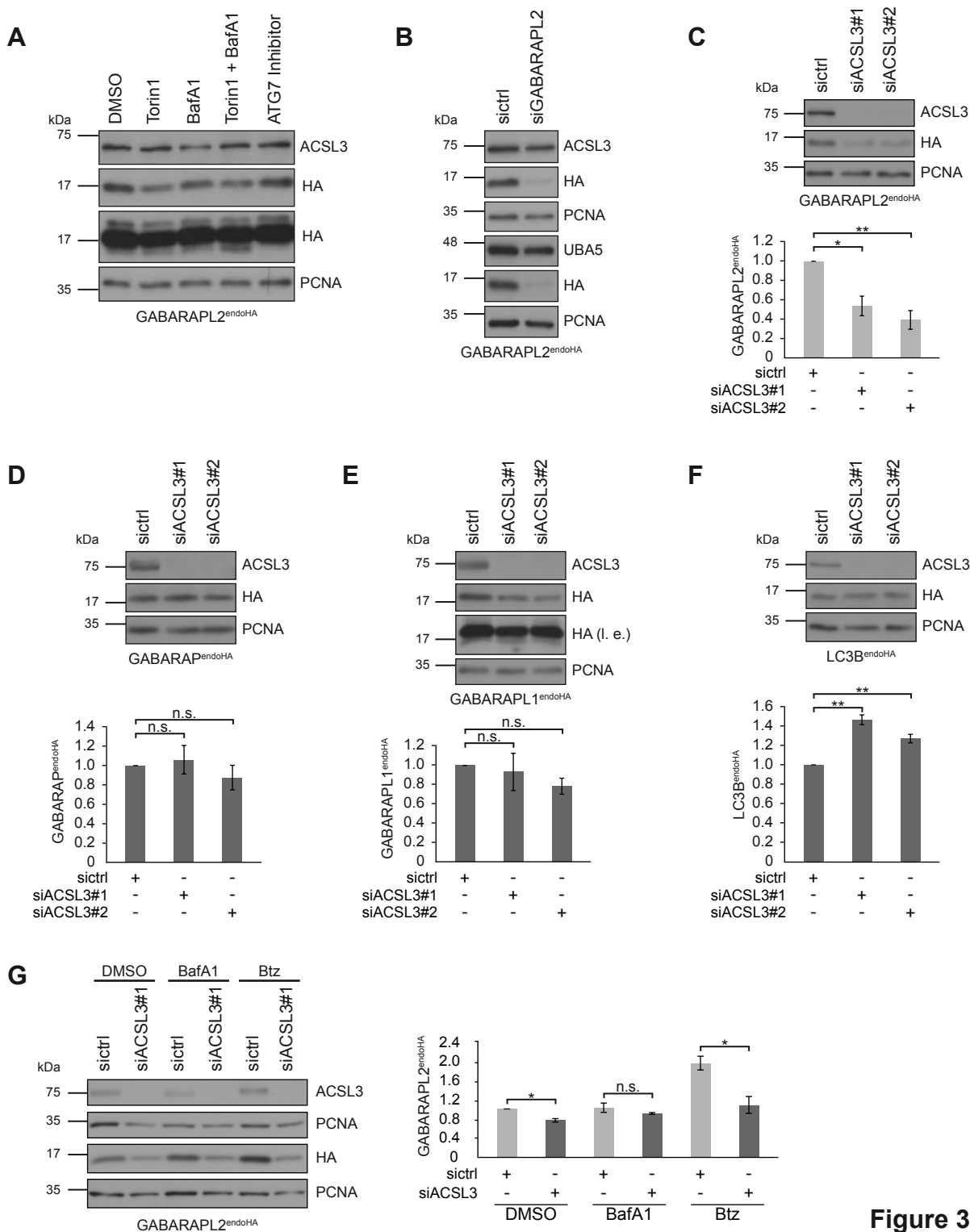
990 **Fig. 8. Oleic acid inhibits ER-phagy.** (A) HeLa cells were transiently transfected with  
991 mCherry-eGFP-RAMP4 and starved with EBSS for 8 hrs in combination with either EtOH or  
992 oleic acid. Red-only puncta were defined as reticulolysosomes. Scale bar: 10  $\mu$ m. Inset scale  
993 bar: 2  $\mu$ m. Arrowheads indicate reticulolysosomes. (B) Quantitative analysis of A. Data  
994 represents mean  $\pm$ SEM. Statistical analysis (n = 3) was performed using Student's t-test  
995 (\*p<0.05). (C) Working model of ACSL3's role in the ufmylation pathway. UBA5 is recruited to  
996 ACSL3 by GABARAPL2. Upon loss of ACSL3 or induction of LD biogenesis ufmylation  
997 components are downregulated and dynamics of UFM1 conjugation are altered. Dotted blue  
998 arrows indicate ER-recruitment, black arrows indicate ufmylation cascade.



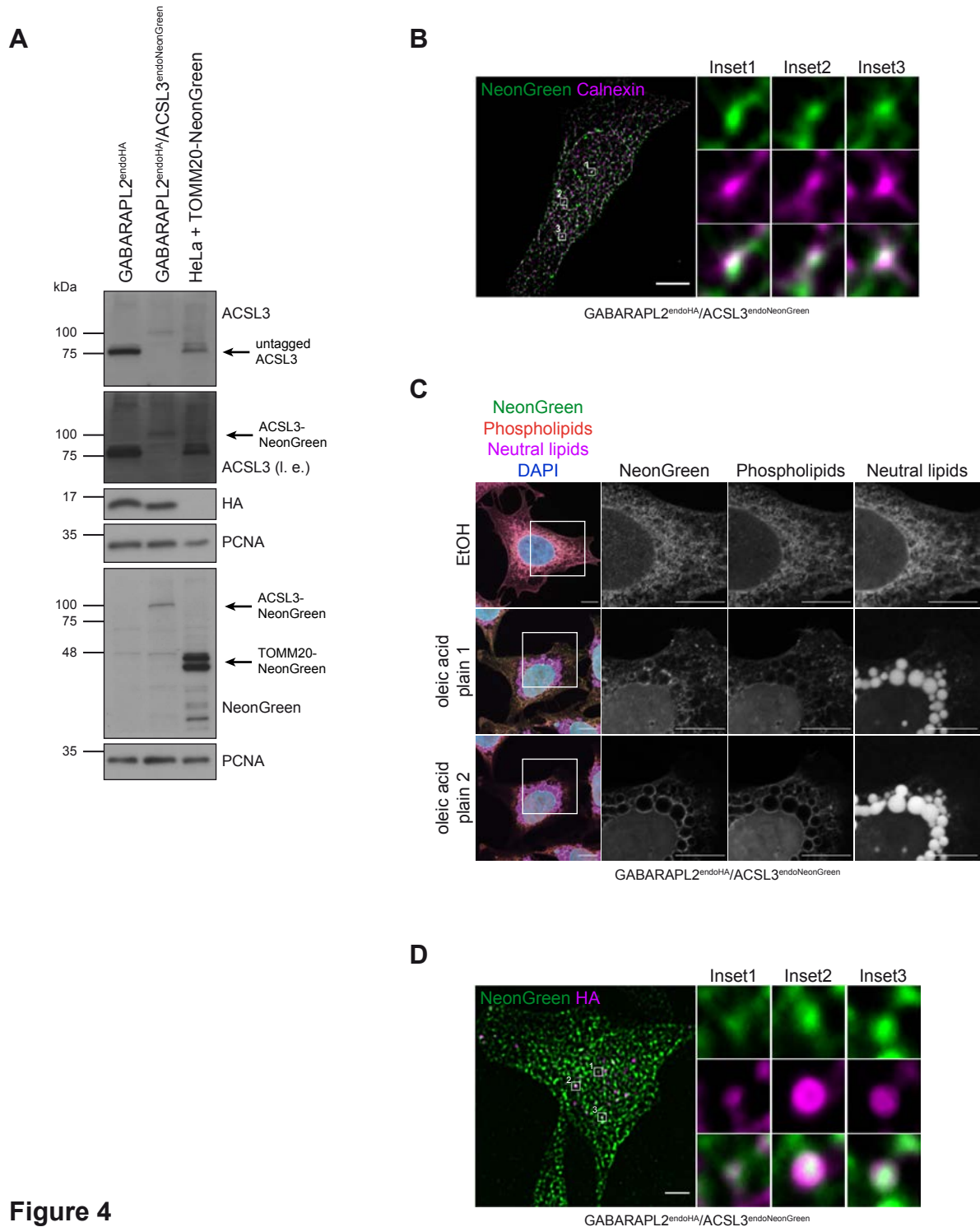


**Figure 1**

**A****B****C****Figure 2**

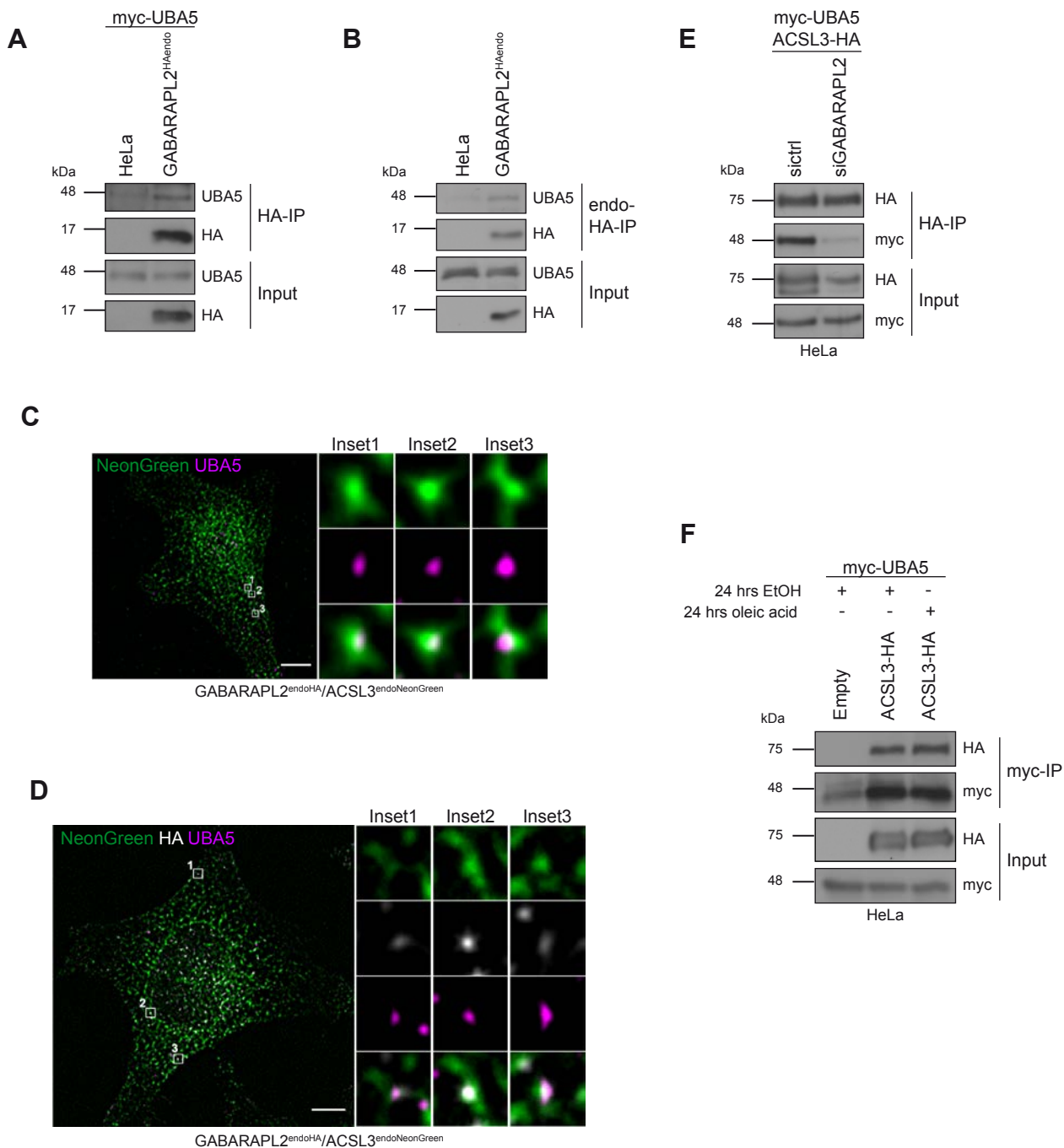


**Figure 3**

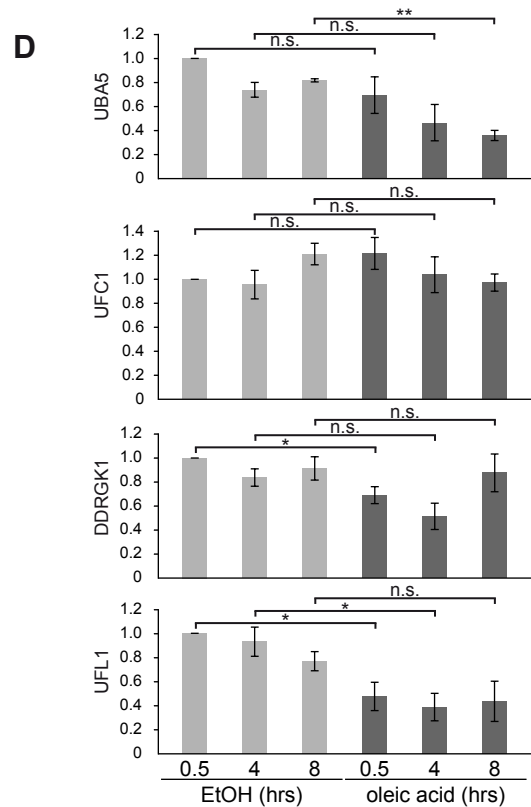
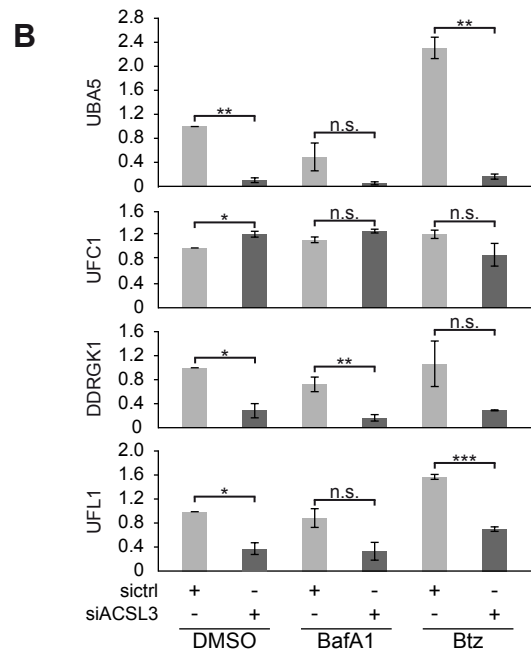
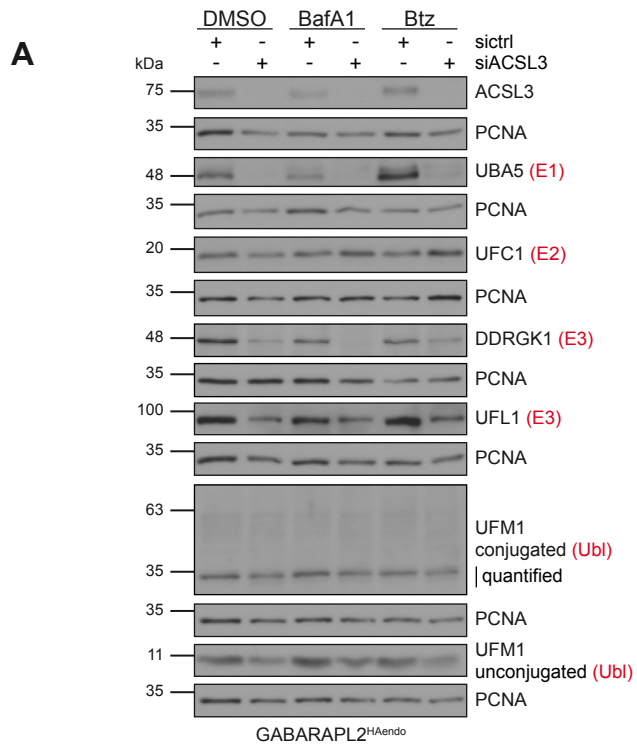


**Figure 4**

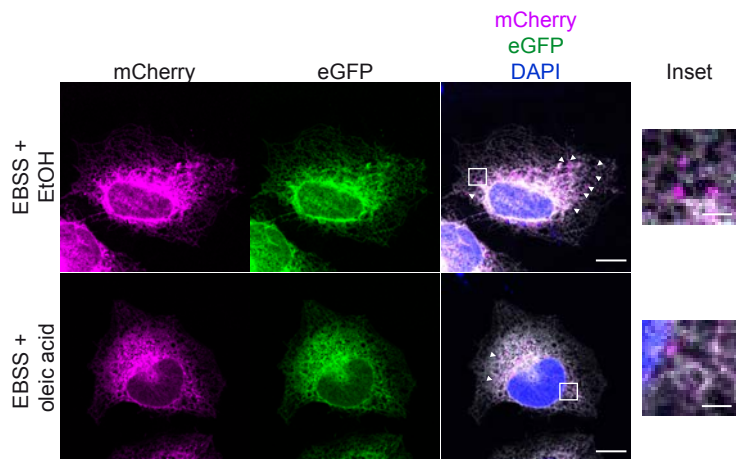
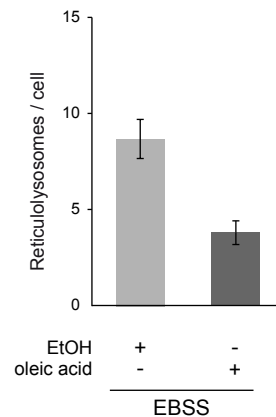
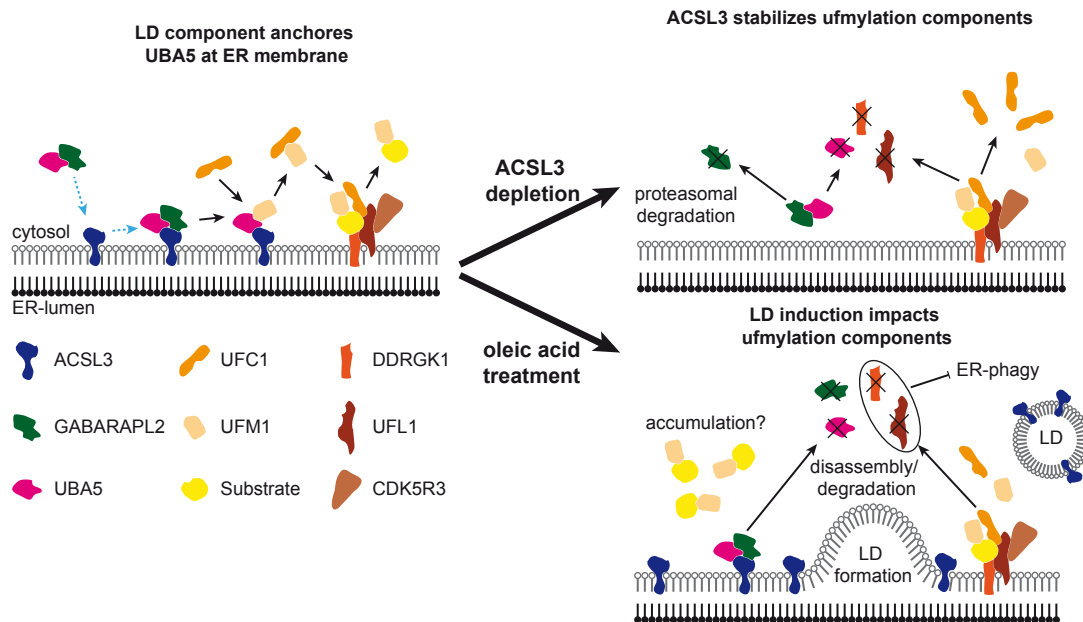




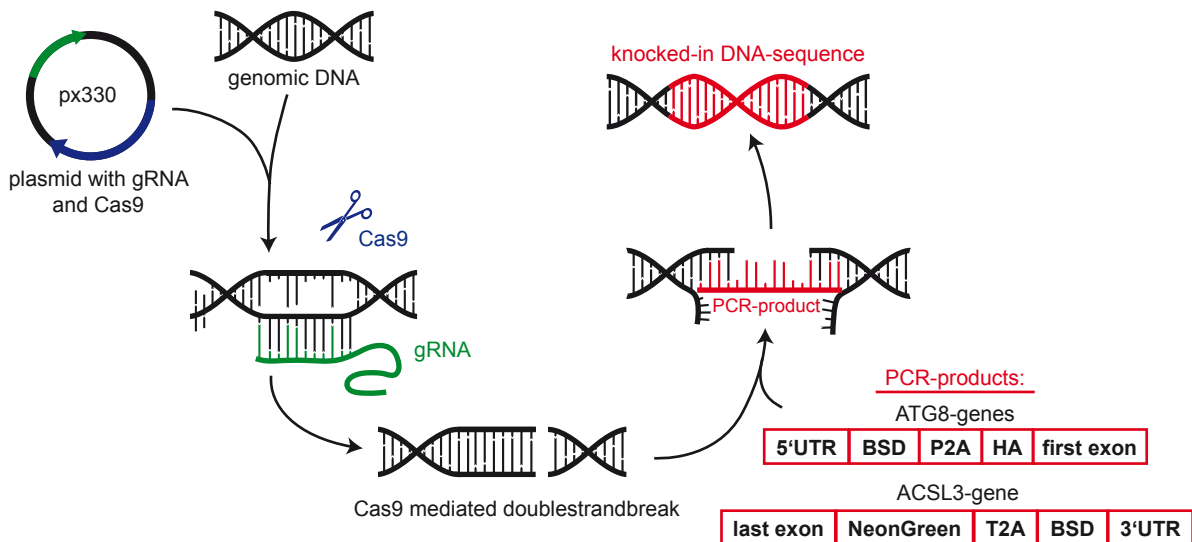
**Figure 6**



**Figure 7**

**A****B****C****Figure 8**



**A****B**

**GABARAP<sup>endoHA</sup>** : TTCGTGGATCGCTCCGCTGAATCCGCCCGCGCGTCGCCGCGCTCGTCGCCGCCCCCGTCCCGGCCCCCTGGGTTCCCTCAGCCCAGCCCTGTCCA  
 GCCCGGTTCCGGGAGGATGAAGCCGGCC**AAGCCTTTGTCTCAAGAAGAATCCACCCTCATTGAAAGAGCAACGGCTACAATCAACAGCATCCCCATCTCTGAAGACTA**  
 CAGCGTCGCCAGCGCAGCTCTCTTAGCGACGGCCGCATCTTCACTGGTGTCAATGTATATCATTTTACTGGGGACCTTGTGCAGAACTCGTGGTCTGGGCACTGCT  
 GCTGCTGCCGACGCTGGCAACCTGACTTGTATCGTCGCGATCGGAAATGAGAACAGGGGCATCTTGAGCCCTCGCGACGGTGCCGACAGGTGCTTCTCGATCTGCATC  
 CTGGGATCAAAGCCATAGTGAAGGACAGTGTGACAGCCGACGGCAGTTGGGATTCGTGAATTGCTGCCCTCTGGTTATGT

**GABARAPL1<sup>endoHA</sup>** : TGCACACTCGGCCAGCGCTGTGGCCCCGAGCGGACGTTTTCTGCAGCTATTCTGAGCACACCTTGACGTCGGCTGAGGGAGCGGGACAGGGTTC  
 AGCGGCGAAGGAGGACAGGCCCGCGCGGGGATCTCGGAAGCGCTGCGGTGCATCAT**GAAGCCGGCCAAAGCTTTGTCTCAAGAAGAATCCACCCTCATTGAAAGAGCAA**  
 CGGCTACAATCAACAGCATCCCCATCTCTGAAGACTACAGCGTCGCCAGCGCAGCTCTCTTAGCGACGGCCGGATCTTCACTGGTGTCAATGTATATCATTTTACTGG  
 GGGACCTTGTGCAGAACTCGTGGTGTGGCACTGCTGCTGCTGCGGCAGCTGGCAACCTGACTTGTATCGTCGCGATCGGAAATGAGAACAGGGGCATCTTGAGCCCT  
 TGCGGACGGTGCCGACAGGTGCTTCTCGATCTGCATCCTGGGATCAAAGCCATAGTGAAGGACAGTGTGACAGCCGACGGCAGTTGGGATTCGTGAATTGCTGCC

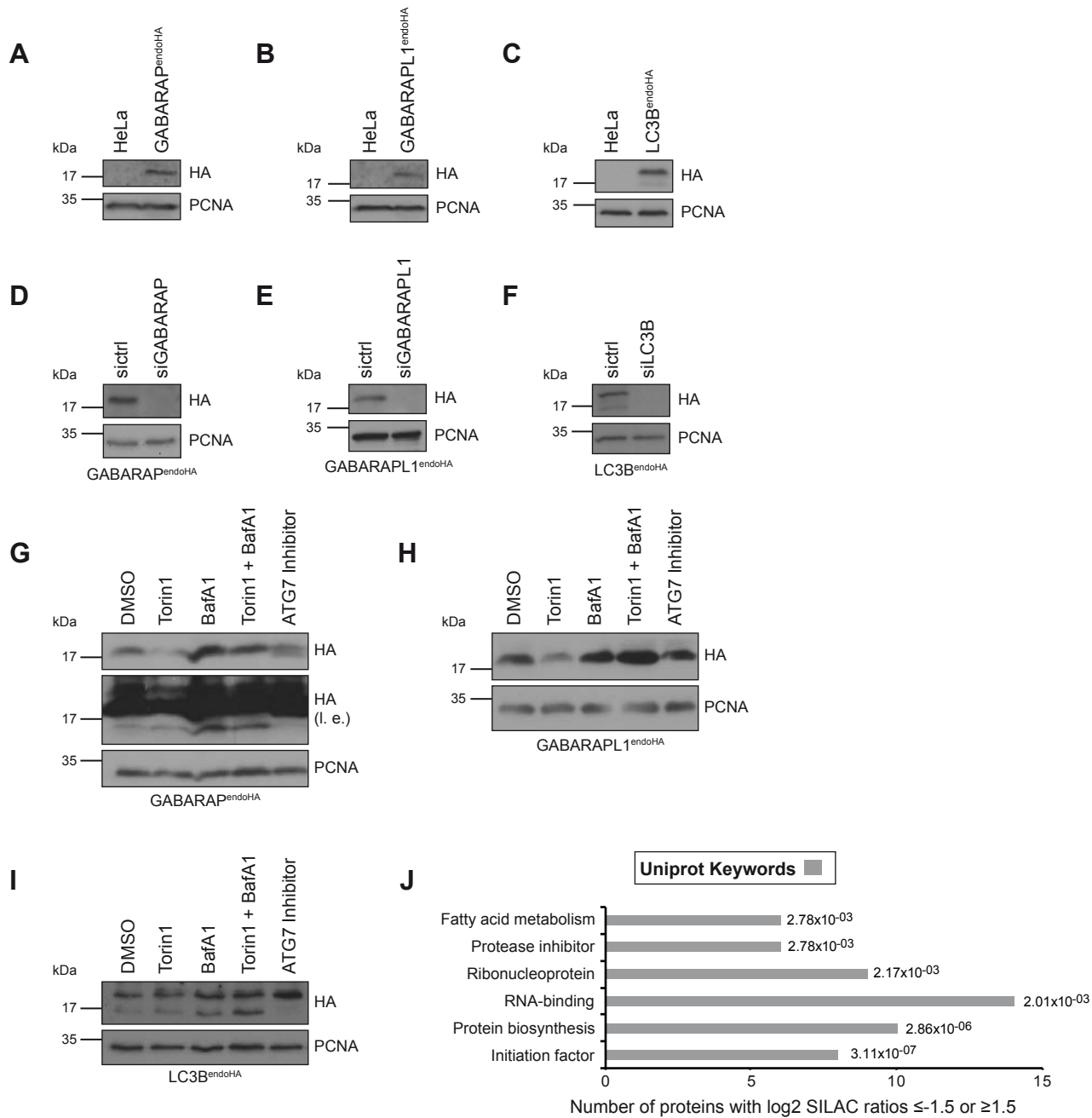
**GABARAPL2<sup>endoHA</sup>** : GCCCCTTTACGTGCGGCCCGCCCTTGGCGTGGCGCCTGACAAATGGCGCCGAAGCCCGCCCGCGCGGTTGCTAGGCTCCGACAGCCGG  
 AAGTCCCGCTGCGGTGTAGTCGCCCGCTCGCTGCCGCTGCCGCGCTCGTGTGTGTTGTGCTCGGTGCGCTGAGCTCCGCGGCTCCGCGAGCCGGTCCGTC  
 CCCTTCCCGCGCGGCCATGAAGCCGGCCAAAGCCTTTGTCTCAAGAAGAATCCACCCTCATTGAAAGAGCAACGGCTACAATCAACAGCATCCCCATCTCTGAAGACTA  
 CAGCGTCGCCAGCGCAGCTCTCTTAGCGACGGCCGCATCTTCACTGGTGTCAATGTATATCATTTTACTGGGGACCTTGTGCAGAACTCGTGGTCTGGGCACTGCT  
 GCTGCTGCCGACGCTGGCAACCTGACTTGTATCGTCGCGATCGGAAATGAGAACAGGGGCATCTTGAGCCCTCGCGACGGTGCCGACAGGTGCTTCTCGATCTGCATC  
 CTGGGATCAAAGCCATAGTGAAGGACAGTGTGACAGCCGACGGCAGTTGGGATTCGTGAATTGCTGCCCTCTGGTTATGTGTTGGGAGGGC

**LC3B<sup>endoHA</sup>** : CTGCGTGCCGCTGCTGGGTTCCGCCACGCCCTCATGGCGGGCCCGCCCGCGGCTCTGGCCCGCCCTCGGTGACGCGTCGCGAGTCACTGACCAGG  
 CTGCGGGCTGAGGAGATACAAGGAAGTGGCTATCGCCAGAGTCGGATTGCGCCGCGCAGCAGCCCGCCCGCCCGGGAGCCCGGGACCTTCGCGTCTGTCGCCCGCC  
 CGCCGCCAGATCCCTGCACCATGCCGGCCAAAGCCTTTGTCTCAAGAAGAATCCACCCTCATTGAAAGAGCAACGGCTACAATCAACAGCATCCCCATCTCTGAAGACT  
 ACAGCGTCGCCAGCGCAGCTCTCTTAGCGACGGCCGCATTTCTACTGGTGTCAATGTATATCATTTTACTGGGGGACCTTGTGCAGAACTCGTGGTGTGGGCACTGCT  
 TGCTGCTGCCGACGCTGGCAACCTGACTTGTATCGTCGCGATCGGAAATGAGAACAGGGGCATCTTGAGCCCTCGCGACGGTGCCGACAGGTGCTTCTCGATCTGCAT  
 CCTGGGATCAAAGCCATAGTGAAGGACAGTGTGACAGCCGACGGCAGTTGGGATTCGTGAATTGCTGCCCTCTGGTTATGTGTTGGGAGGGC

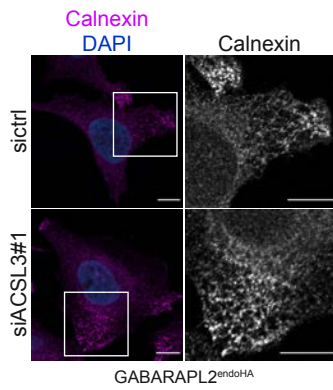
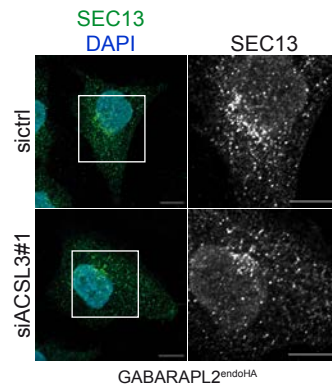
**C**

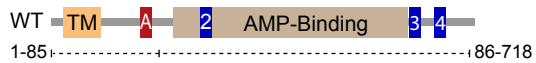
**ACSL3<sup>endoNeonGreen</sup>** : TATTTTTTTTTAATCATCTTAGCAAGTCTGGAAAAGTTGAAATTCAGTAAAAATTCGTTTGTAGTCATGAACCGTGGACCCCTGAAACTGGTCT  
 GGTGACAGATGCCTTCAAGCTGAAAACGCAAGAGCTTAAAACACATACCAGCGGACATTTGAGCGAATGTATGGAAGAAAAGCTGGCGGCATGGTGGACAGGGCCGAG  
 GAGGATAACATGGCCCTCTCTCCAGCGACACATGAGTTACACATCTTTGGCTCCATCAACGGTGTGGACTTTGACATGGTGGGTGAGGGCACCGGCAATCCAATGATG  
 GTTATGAGGAGTTAAACCTGAAGTCCACCAAGGGTGACCTCCAGTTCTCCCCCTGGATTCTGGTCCCTCATATCGGGTATGGCTTCCATCAGTACCTGCCCTACCCTGA  
 CGGGATGTGCGCTTTCCAGGCCCATGTTAGTAGTGGCTCCGGATACCAAGTCCATCGCAATGCAGTTTGAAGATGGTGCCT

**Figure S1**



**Figure S2**

**A****B****Figure S3**

**A**

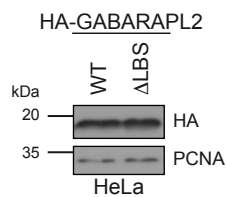
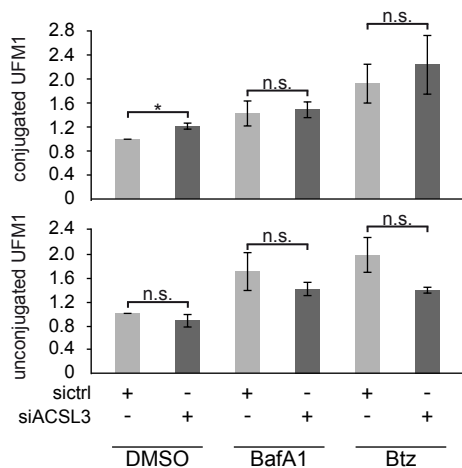
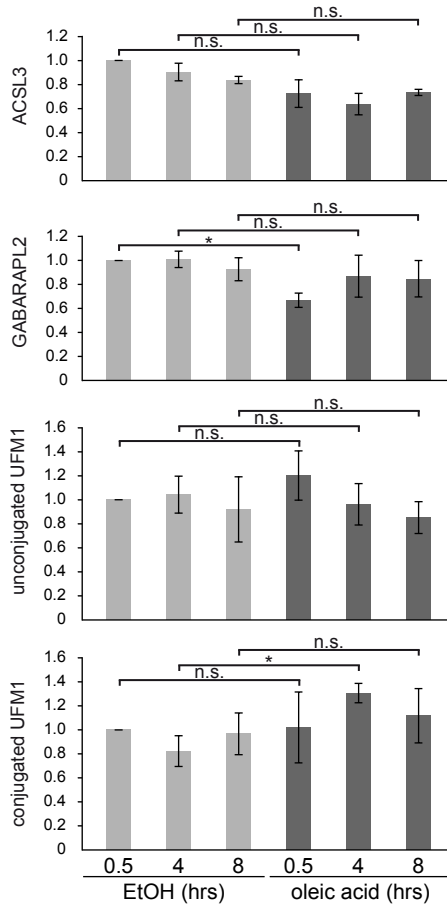
potential LIR potential UIM

**LIR-2** (135-140): LSYEDV

**LIR-3** (589-594): GEYVSL

**LIR-4** (643-648): GTWEEL

**UIM-A** (72-81): SLDGLASVL

**B****C****D****Figure S4**

## 1 **Supplementary figure legends**

2 **Fig. S1. Endogenous epitope tagging of hATG8 and ACSL3 genes.** (A) Experimental  
3 CRISPR/Cas9 workflow. (B,C) Sequence data from PCR products of the tagged  
4 GABARAP<sub>endoHA</sub>, GABARAPL1<sub>endoHA</sub>, GABARAPL2<sub>endoHA</sub>, LC3B<sub>endoHA</sub> cell lines (B) and the  
5 GABARAPL2<sub>endoHA</sub>/ACSL3<sub>endoNeonGreen</sub> cell line (C). Introduced CRISPR sequences are  
6 indicated in bold.

7

8 **Fig. S2. Validation of endogenously HA-tagged hATG8 proteins.** (A-C) GABARAP<sub>endoHA</sub>  
9 (A) GABARAPL1<sub>endoHA</sub> (B) LC3B<sub>endoHA</sub> (C) and parental HeLa (A-C) cells were lysed followed  
10 by immunoblotting and analysis with indicated antibodies. (D-F) GABARAP<sub>endoHA</sub> (D),  
11 GABARAPL1<sub>endoHA</sub> (E), LC3B<sub>endoHA</sub> (F) cell lines were reversely transfected with indicated  
12 siRNAs prior to immunoblot analysis. (G-I) GABARAP<sub>endoHA</sub> (G), GABARAPL1<sub>endoHA</sub> (H),  
13 LC3B<sub>endoHA</sub> (I) were treated as indicated followed by lysis and immunoblotting. (J) Annotation  
14 enrichment analysis of candidate GABARAPL2-interacting proteins with log<sub>2</sub> SILAC H/L ratios  
15  $\geq 1.5$  or  $\leq -1.5$ . The bar graphs show significantly overrepresented UniProt keywords.

16

17 **Fig. S3. ACSL3 is not an autophagy substrate.** (A,B) GABARAPL2<sub>endoHA</sub>/ACSL3<sub>endoNeonGreen</sub>  
18 cells were transfected with indicated siRNAs prior to immunolabeling with Calnexin (A) or  
19 SEC13 (B). Scale bar: 10  $\mu$ m.

20

21 **Fig. S4. Effects of ACSL3 depletion and LD induction on ufmylation.** (A) Amino acid  
22 sequences of potential LIRs and UIM in ACSL3. (B) Immunoblot analysis of HeLa cells stably  
23 expressing wild-type (WT) and LIR-binding deficient ( $\Delta$ LBS) GABARAPL2. (C) Quantitative  
24 analysis from Fig. 7A. Data represents mean  $\pm$ SEM. Statistical analysis (n = 3) of the indicated  
25 protein/PCNA ratio normalized to sictrl-DMSO was performed using Student's t-test (\*p<0.05,  
26 \*\*p<0.01, \*\*\*p<0.001). (D) Quantitative analysis of Fig. 7C. Data represents mean  $\pm$ SEM.  
27 Statistical analysis (n = 3) of the indicated protein/PCNA ratio normalized to 0.5 hrs EtOH was  
28 performed using Student's t-test (\*p<0.05, \*\*p<0.01).